The Influence of Particle Size on the Chemistry of Mica Clays

by

Paul Lawrence Gassman

Thesis submitted to the Faculty of the

Virginia Polytechnic Institute and State University

in partial fulfillment of the requirements for the degree of

Master of Science

in

Crops and Soil Environmental Sciences

APPROVED:

Lucian W. Zelazny

F. Donald Bloss

James C. Baker

William J. Edmonds

February, 1990

Blacksburg, Virginia

c.2

LD
5655
V855
1990
G383
c.2

The Influence of Particle Size on the Chemistry of Mica Clays

by

Paul Lawrence Gassman

Lucian W. Zelazny

Crops and Soil Environmental Sciences

(ABSTRACT)

In order to assess the importance of particle size on elemental composition, structure, morphology, and charge characteristics of 2:1 micas, mechanically produced clay separates were analyzed by; electron probe microanalysis (EPMA), transmission electron microscopy (TEM), thermogravimetry, specific surface area analysis, and ion exchange. Books of biotite and muscovite were reduced to clay size (<2.0 μm) particles by mechanical comminution, then further fractionated into coarse (0.2-2.0 μm), medium (0.08-0.2 μm), and fine (<0.08 μm) clay sizes. Composition of the clay size micas was particle size dependent, compositional changes being smaller for the medium and coarse clays. Grinding produced significant losses of interlayer K, decreased crystallinity, but increased water content as particle size decreased.

The medium and coarse clays maintained coherent basal diffractions, wheras, significant peak broadening of x-ray diffraction maxima was observed for the fine clays. Diffracted peak broadening was due to the reduced crystallite size and the semirandom orientatition of lath shaped particles.

Specific surface area, adsorbed water, and structurally coordinated water increased as particle size decreased. Specific surface areas were determined by adsorption of molecular nitrogen, at liquid nitrogen tempertures. The increased water contents were measured by thermogravimetric analysis.

An increase in CEC of the muscovite clays was detected with decreasing particle size, increasing solution pH, and increasing ionic strenth. Assignment of specific exchange capacities for the three clays was confounded by Al hydrolysis and depressed solution pH.

Acknowledgements

My most sincere appreciation goes to my wife, Carol, whose patience, support, and understanding enabled me to devote my energies to my professional development. Carol has also given me previously unfathomable joy with the birth of our son Clayton, who also provided me with the energies to complete my degree requirements.

Heartfelt appreciation also goes to my chairman, Lucian Zelazny whose considerable efforts as a professor and as a supervisor have given me valuable personal and professional experiences. I had the pleasure of working in one of the best equipped labs in the United States in clay mineralogy and soil chemistry. I would also like to thank the other members of my committe: Dr. F. Donald Bloss, Dr. James C. Baker, and Dr. William J. Edmonds for their valuable contributions to my research efforts, the preparation of my thesis, and for their patience with my progress as a part-time student.

The assistance of Todd Solberg in the electron microprobe analyses was greatly appreciated, particularly in view of the time savings realized through his expertise, and the quality of the analytical data. Thanks are also due to Dr. Paul Ribbe for availing to me the microprobe facilities of the Department of Geological Sciences. Gratitude is also extended to my wife,

Carol, for her professional assistance with electron microscopic analyses of my samples, and to Dr. David Stetler for the use of the microscope.

Appreciation is also extended to my inlaws, the Stapletons, for their support.

Table of Contents

Introduction 1

Literature Review 4

Methods 11

Results 18

Discussion 69

Literature Cited 78

Vita 82

List of Illustrations

Figure 1. Transmission electron micrographs of the fine clays (<0.08 μm) of a) biotite and b) muscovite. Bars = 1 μm 27

Figure 2. Transmission electron micrographs of the medium clays (0.08-0.2 μm) of a) biotite and b) muscovite. Bars = 1 μm 28

Figure 3. Transmission electron micrographs of the coarse clays (0.2-2.0 μm) of a) biotite and b) muscovite. Bars = 1 μm 29

Figure 4. Distribution of particle heights measured by electron microscopy for the fine clays of biotite and muscovite. 30

Figure 5. Distribution of particle heights measured by electron microscopy for the medium clays of biotite and muscovite. 31

Figure 6. Distribution of particle heights measured by electron microscopy for the coarse clays of biotite and muscovite. 32

Figure 7. Distribution of basal areas measured by electron microscopy for the fine clays of biotite and muscovite. 33

Figure 8. Distribution of basal areas measured by electron microscopy for the medium clays of biotite and muscovite. 34

Figure 9. Distribution of basal areas measured by electron microscopy for the coarse clays of biotite and muscovite. 35

Figure 10. X-ray diffractogram of the extremely broad and weak 10Å peak of fine clay muscovite. 38

Figure 11. X-ray diffractogram of fine clay muscovite from 2 to 32 degrees 2Θ, exhibiting very weak diffraction maxima. 39

Figure 12. X-ray diffractogram of medium clay muscovite possessing weak nonbasal and strong basal reflections. 40

Figure 13. X-ray diffractogram of coarse muscovite clay exhibiting strong basal and nonbasal reflections at all temperatures. 41

Figure 14. X-ray diffractogram of the 10Å peak of coarse muscovite displaying the heat induced reduction of intensity. 42

Figure 15. X-ray diffractogram of the extremely broad and weak basal reflections of fine clay bioitite. 43

Figure 16. X-ray diffractogram of medium clay biotite exhibiting heat dependent changes in peak intensities. 44

Figure 17. X-ray diffractogram of coarse clay biotite exhibiting heat dependent changes in peak intensities. 45

Figure 18. X-ray diffractogram of the 10Å peak of coarse clay biotite displaying the collapse of basal spacing with heating. 46

Figure 19. Composite thermogram of weight losses of muscovite clays due to desorption and dehydroxylation. 49

Figure 20. Composite thermogram of weight losses of biotite clays due to desorption and dehydroxylation. 50

Figure 21. Composite cation exchange curve of Na^+ in 0.1N NaCl as influenced by the clay size of muscovite. 53

Figure 22. Composite cation exchange curve of Na^+ in 0.01N NaCl as influenced by the clay size of muscovite. 54

Figure 23. Composite cation exchange curve of Na^+ in 0.001N NaCl as influenced by the clay size of muscovite. 55

Figure 24. Composite cation exchange curve of interlayer K^+ in 0.1N NaCl as influenced by the clay size of muscovite. 57

Figure 25. Composite cation exchange curve of interlayer K^+ in 0.01N NaCl as influenced by the clay size of muscovite. 58

Figure 26. Composite cation exchange curve of interlayer K^+ in 0.001N NaCl as influenced by the clay size of muscovite. 59

Figure 27. Composite cation exchange curve of Al^{3+} in 0.1N NaCl as influenced by the clay size of muscovite. 60

Figure 28. Composite cation exchange curve of Al^{3+} in 0.01N NaCl as influenced by the clay size of muscovite. 61

Figure 29. Composite cation exchange curve of Al^{3+} in 0.001N NaCl as influenced by the clay size of muscovite. 62

Figure 30. Composite cation exchange curve of "exchangeable" H^+ in 0.1N NaCl as influenced by the clay size of muscovite. 63

Figure 31. Composite cation exchange curve of "exchangeable" H^+ in 0.01N NaCl as influenced by the clay size of muscovite. 64

Figure 32. Composite cation exchange curve of "exchangeable" H^+ in 0.001N NaCl as influenced by the clay size of muscovite. 65

Figure 33. Composite anion exchange curve of Cl^- in 0.1N NaCl as influenced by the clay size of muscovite. 66

Figure 34. Composite anion exchange curve of Cl^- in 0.01N NaCl as influenced by the clay size of muscovite. 67

Figure 35. Composite anion exchange curve of Cl^- in 0.001N NaCl as influenced by the clay size of muscovite. 68

List of Tables

Table 1. Weight percent oxides of muscovite clays and sheets determined by electron probe microanalysis (H_2O calculated). 19

Table 2. Weight percent oxides of biotite clays and sheets determined by electron probe microanalysis (H_2O calculated). 20

Table 3. Stoichiometric half-cell formulas of muscovite and biotite clays and sheets, allocated by the program SuperRecal. 21

Table 4. Water contents calculated by SuperRecal and those measured by Thermogravimetric analyses. 22

Chapter I

Introduction

Micas are an important primary and secondary mineral component in both geologic and soil systems. The ability of soil micas to fix K in the interlayer of the 2:1 layers and their nearly ubiquitious distribution make them a very important mineral group. The exchange of K from micas by soil solutions initiates significant changes in their composition and structure. Removal of interlayer K and particle dissolution may be coupled in the weathering reactions of soil micas. Often accompanying mica weathering is the reduction of particle size which induces shifts in the sites of charge and rearrangements of the crystalline lattice.

To examine the influence of fine particle size on the crystallochemical characteristics of micas, clay size separates of muscovite and biotite were prepared. These mica clays were produced by the mechanical comminution of book muscovite and book biotite. The mica books were ground to produce three clay size particle separates; 0.2-2.0 μm., 0.08-0.2 μm, and <0.08 μm. These clay separates were characterized mineralogically by electron probe microanalysis (EPMA), transmission electron microscopy (TEM), x-ray diffraction (XRD), thermogravimetry, ion exchange, and specific surface area analysis.

Muscovite and biotite were chosen to represent typical dioctahedral and trioctahedral micas occurring in soils, respectively. Muscovite is relatively more resistant to weathering than biotite. Muscovite, a dioctahedral 2:1 phyllosilicate, consists of two tetrahedral sheets enclosing a single octahedral sheet. The octahedral sheet contains Al in two of the three crystallographically unique positions in each unit cell, thereby being designated dioctahedral. The tetrahedral sheets contain corner-sharing Si tetrahedra, which form pseudohexagonal siloxane rings. These sheets of tetrahedrally coordinated Si are bonded to the octahedral sheet by the apical oxygens of the tetrahedra. The enclosing tetrahedral sheets articulate to the octahedral sheet, producing the pseudohexagonal rings and a corrugation of the basal tetrahedral surfaces. The ideal half-cell formula of muscovite is $K[Al_2][Si_3Al]O_{10}(OH)_2$, with the substitution of an Al ion for Si in the tetrahedral sheet. This substitution creates an electrostatic charge imbalance (-1), compensated for by the coordination of K in the interlayer of 2:1 layers.

Biotite, also a 2:1 phyllosilicate, differs from muscovite by being trioctahedral. The three octahedral positions are filled by divalent Fe and or Mg. The half-cell formula of an ideal biotite, $K[Mg,Fe]_3[Si_3Al]O_{10}(OH)_2$, indicates more elemental variability within the crystal structure than in muscovite. These ideal formulas for muscovite and biotite are rarely if ever found in natural systems. The degree of crystalline perfection and elemental purity of micas is dependent on the genetic history of the mineral, particularly in the mixed mineral system of soils.

Examination of the clay separates indicates significant changes in composition and crystallinity associated with decreasing particle size. As particle size decreases, so does K content, percentage of tetrahedrally coordinated Al, and coherence of x-ray diffraction maxima. As expected, the specific surface area and the amount of coordinated water increases as the size of the clay decreases. Transmission electron microscopy of the fine clays suggests a propensity towards lath morphology. Measurements of the cation exchange capacity of the muscovite clays indicates an increase in pH dependent charge with decreasing

particle size, as proportionally more edge area is exposed to exchange by the finer particle sizes.

Chapter II

Literature Review

Electron probe microanaysis

The use of electron probe microanalysis for the quantitative chemistry of small particles can provide accurate and precise data, provided that the limitations are known and appropriate correction factors used.

The analysis of clay size (<2.0 μm) materials presents a challenge to microbeam quantification, particularly for elements of low abundance. The potential problems associated with microbeam analysis of particles smaller than the electron beam are greater than for macroparticles. In most instances, the established mathematical corrections (ZAF) for atomic number (Z), absorption (A), and x-ray fluorescence (F) are applicable to small particle analysis (Heinrich, 1981). In a thorough theoretical treatment of small particle analysis, by Armstrong and Buseck (1975), the corrections for quantitative analysis due to particle size and or particle shape were discussed. Both particle size and particle shape influence; the backscatter of electrons, the depth distribution of x-ray production, x-ray path length, and characteristic fluorescence from within the sample. Armstrong and Buseck suggest that backscattered

electrons represent a small error when data is normalized, and that sample fluorescence may be corrected with the conventional correction factor. Of the potential errors, they indicate that the most critical correction is for particle shape and size effects on the x-ray path length. These authors provide particle geometry models to correct for the x-ray path length component of the absorption correction. Also presented was a correction for the less serious variations of depth distribution of x-ray generation. Other potential sources of analytical error of small particles are backscattering of electrons and x-ray emission from the sample substrate (Heinrich, 1981). These errors occur when the excitation volume is greater than the sample dimensions, and they may be eliminated by using thin film or low atomic number substrates. Sample homogeneity and distribution of mass within particles are also important factors in the analysis of both macro and micro particles. Heinrich also dicussed the importance of precise focusing of the sample for quantitative work.

Microbeam analysis of mica samples poses other potential problems which include; significant effects of particle orientation and mass distribution, lateral diffusion of electrons within particles, and diffusion of alkali elements. Van der Pluijm et al. (1988) observed the diffusion of K from micas to be dependent on particle orientation. These authors observed the mottling of mica sheets due to irradiation, which according to Ahn et al. (1986) was due to lateral diffusion of K. Deleterious effects of particle shape and orientation effects are reduced when the electron beam diameter is larger than the particle diameter. However, these effects can not be discounted because particles at the edge of the excitation volume will affect the absorption function. Mackinnon and Kaser (1987) presented a method of reducing analytical errors of clays due to beam induced element loss. Their experiments on well-crystalline Georgia kaolinite suggest that element loss can be minimized at low temperatures (-150 °C).

Transmission electron microscopy

Electron microscopy has been very useful in the field of clay mineralogy where particle sizes are below the resolving power of light microscopy. The value of electron microscopy lies its ability to supply morphological, chemical and structural details about clays. The merits of electron imaging and analysis to clay mineralogy were discussed by Bates (1964). Numerous investigators have used the morphologic capabilities of this instrument in weathering and ion exchange studies, and to detect interstratification. Differentiation of clay polytypes, particularly the micas, may be performed on those instruments equipped with selected area diffraction (SAD) goniometers. A thorough treatment of the application of electron microscopy in clay mineralogy is beyond the scope of this discussion, and the interested reader is referred to noteable texts on this subject by; Heidenreich (1964), Beutelspacher and van der Marel (1968), and Suito and Nakahira (1971).

X-ray diffraction

The identification of clay minerals by x-ray diffraction is performed by recognition of the characteristic diffraction maxima. Grim (1968) provides a thorough discussion of the use of XRD for the identification and characterization of many clay minerals. The more current text by Brown and Brindley (1980) includes the x-ray characterization of the common phyllosilicates, complex clay mineral mixtures and interstratified minerals.

The identification of mica minerals by XRD is based on the recognition of the diffraction maxima at 10, 5, and 3.3 Å, dependent on the mica species. Generally, trioctahedral micas with high Fe contents do not exhibit a 5.0 Å peak. Conversely, the aluminuous dioctahedral micas possess a strong 5.0 Å peak. Distinction of dioctahedral and trioctahedral micas may be performed by determining the 060 spacing. In dioctahedral minerals the 060 spacing is

smaller than for trioctahedral minerals, due to occupancy of only two octahedral sites. Diffraction analysis of randomly oriented specimens may be used to distinguish the layer stacking sequence of clays, particularly, the polytypic micas.

The diffraction characteristics of the mica clays were predictably in accord with expected behavior. The most prominent feature of the clays was the broadening of diffraction peaks with decreasing particle size (Cullity, 1968). Cullity considered a small particle of an otherwise perfect crystal as being a crystal imperfection. The small particle size produces a scattering of diffracted rays, thereby broadening the coherent diffracted rays. Another interference to precise (ideal) diffraction is the presence of mosaic structure. Cullity describes this crystal imperfection as a small angular misalignment of 1000Å lattice blocks within the crystal, which produces significant broadening of diffraction peaks. Several other instrument and specimen characteristics which affect x-ray diffraction are discussed by Cullity, and the interested reader should refer to his text.

Thermogravimetric analysis

The thermal behavior of micas are dependent on their composition, stacking sequence, particle size, and degree of crystallinity. The amount of adsorbed moisture on the surface of clays is dependent on the particle size, surface area and degree of crystallinity (Grim, 1968). Most adsorbed water is evolved from the clay surface below 300 to 350°C. Thermogravimetric analysis (TGA) of micas is dominated by the evolution of the ligand (OH). This dehydroxylation occurs as the O-H bonds in the octahedral postions are broken, and H is volatilized with O. The temperature at which dehydroxylation occurs varies with mica species (Mackenzie, 1970), and with octahedral cation. Magnesium-rich micas have higher dehydroxylation temperatures than aluminous micas, and aluminous micas higher than ferrous (Jackson, 1969). The dioctahedral micas lose hydroxyls between 400 and 800°C and at 1100°C recrystallize as corundum, leucite and cristobalite (Mackenzie, 1970). Biotite dehydroxylates in the same

range as dioctahedral minerals, however, the oxidation of Fe^{2+} during heating may produce a weight increase. Overlapping of this oxidative weight gain during dehydroxylation confounds determination of the true weight loss. At 1100°C biotite recrystallizes as iron rich spinel, leucite, and mullite (Roy, 1949). Bradley and Grim (1951) showed that the temperature of dehydroxylation of muscovite decreased as particle size decreased, and that the temperature range of dehydroxylation broadened.

Specific surface area analysis

The isothermal adsorption of gases was first mathematically described by Langmuir (1918). His theoretical equations were used to describe the adsorption of various gases on the surfaces of glass, mica, and platinum. An improved theoretical treatment was provided by Brunauer, Emmett, and Teller (BET) (1938), which accounted for deviations from ideal Langmuir behavior. Use of the BET mathematical treatment enabled distinction between monolayer and multilayer adsorption. Surface areas of the muscovite and biotite clays were determined with the adsorption of purified nitrogen, and the BET data treatment.

Ion exchange measurements

The influence of particle size on cation exchange characteristics of micas has been examined by von Reichenbach and Rich (1969). They prepared ground muscovite to examine the rate of K release, finding that larger particles release proportionally more K than smaller particles. These authors suggested that smaller particles have a higher ion selectivity for K. This higher selectivity was attributed to a lesser degree of bending at particle edges, than that found on coarser particles. Mackenzie and Milne discussed the effects of grinding on the cation exchange, thermal and x-ray diffraction properties of biotite and vermiculite (1951) and muscovite (1953). According to Mackenzie and Milne the CEC of muscovite and biotite in-

creases with grinding time. The effect of grinding on vermiculite was inconclusive, sometimes the CEC was slightly higher and at others lower than the initial exchange capacity. Baweja et al. (1974) examined the influence of particle size reduction on the CEC of Libby vermiculite, the CEC decreasing with increasing grinding time. The conversion of vermiculite to hydrobiotite by grinding caused the lowering of the CEC.

In addition to particle size effects, particle edge structure has been shown to influence ion exchange from micas. The influence of the crystal structure at the edge of mica particles was shown to alter the rate of K diffusion from phlogopites (Newman and Brown, 1969). They showed that the creation of a very smooth particle edge by an air jet dramatically reduced the rate of diffusion. Raman and Jackson (1965), using sodium tetraphenylboron (NaTPB) to diplace interlayer K from biotite, detected the rolling of particle edges. They also suggested that weathering, largely by the formation of surface cleavages and cracks, occurred at basal mica surfaces. The cleavage and surface cracks created fresh edges for K removal. Huff (1972) also used NaTPB to create particle fractures and particle splinters during K removal from illite and illite-montmorillonite. Huff suggested that particle splintering increased surface area, due to the release of lattice stresses during K removal.

Conflicting evidence exists as to the importance of solution pH in the ion exchange reactions of micas. Scott and Smith (1966) noted that the removal of interlayer K from illite was not dependent upon the hydrogen ion concentration between pH 4.6-9.2. A comparison of the effectiveness of K removal by several Na salts at various pH values was made by Wells and Norrish (1968). They reported that removal of interlayer K was insensitive to the hydrogen ion concentration, protons behaving much like a metal cation. Conversely, Lin and Clemency (1981) found that release of K and Na from dry-ground muscovites was enhanced by hydrogen ions in solution. Two thirds of the K released was attributed to release from internal structural positions. Raman and Jackson (1966) also investigated the pH dependence of K removal from micas. They found that the extraction of K from muscovite was enhanced at lower pH values. During K replacement they observed an increase in solution pH, causing them to surmise the

coordination of protons to oxygens in the tetrahedral layer. Newman (1970) examined the influence of hydrogen ions on K exchange in eleven trioctahedral micas. He ascertained that exchange was enhanced by increased proton concentration. He also recognized that a rise in solution pH was circumstantial evidence for protons being incorporated into the aluminosilicate structure.

Several researchers have examined the influence of the exchange salt on the cation exchange characteristics of micas. Boiling solutions of NaCl, $MgCl_2$, acetic acid, sodium citrate, and molten lithium nirate were utilized by Cook and Rich (1963) to artifically weather muscovite. The boiling chloride and acetic acid solutions produced small changes in the CEC of the mica, and the chloride salts promoted interlayer expansion. The sodium citrate extraction increased the CEC due to Al complexation, which released adsorbed polymeric Al from exchange sites. The molten lithium nitrate treatment produced the largest increase in CEC. Molten lithium nitrate effectively removes interlayer K. Potassium removal allows Li to migrate into octahedral positions causing changes in the lattice spacings of micas.

Chapter III

Methods

Mechanically produced clays were prepared by grinding book specimens of muscovite and biotite. Grinding of the mica books produced clay separates of fine (<0.08 μm), medium (0.08-0.2 μm), and coarse (0.2-2.0 μm) particle sizes. Mineralogical characterization of the monomineralic clay separates of muscovite and biotite were performed. The use of ground clay caused concern about the destruction of the natural crystal structure and alteration of crystal chemistry. It was anticipated that the comminution of particles by knife blades may alter edge sites, and possibly cause long range distortion of interlayer cation and hydroxyl sites. There was also concern about the production of noncrystalline material as particles were cleaved.

Sample preparation

Clay size micas were prepared from pegmatitic book muscovite from Lord Hill, Stoneham, Maine (Wards Scientific) and pegmatitic biotite from the Silver Crater Mine, Bancroft, Ontario (VPI & S.U., Geology Museum). Sheets from the book micas were separated into thin folia by

splitting with razorblades. The folia were optically examined for impurities and cut with scissors to remove contaminants. These optically clean sheets were briefly dry-ground in a blender, and transferred to an Omni Corporation (Sorvall) homogenizer (a stainless steel jar and knife blade assembly). Approximately 25 grams of ground mica was placed in the homogenizer and 200 ml of deionized-distilled water added. The homogenizer jar with sample and solution was immersed in a controlled water bath at 10°C, and was allowed to equilibrate for 20 minutes prior to grinding. The water bath effectively maintained the temperature of the sample during grinding, eliminating concerns about thermal degradation of particles. The homogenizer was operated at approximately 7500 rpm for up to 20 hours. The production of clay size material was exceedingly slow and inefficient, so the blade assembly of the homogenizer was replaced by a generator. The generator is an impeller driven cutter with extremely sharp castellated teeth. The generator is usually used to mince biological materials, and as such was subjected to extreme conditions in this application. Although muscovite has a Moh's hardness of 2.0 to 2.5, it proved to be extremely resilient to mechanical cutting and grinding. The generator was more efficient at reducing the particle size than the homogenizer. An estimate of the turn over rate for fine clay ($<0.08\mu m$) production was approximately 100 mg for 80 hours grinding of starting material. The sample solution was removed and the particles separated by centrifugation and decantation into fine, medium and coarse clay sizes. Material larger than $2\mu m$ was returned to the homogenizer for continued comminution. The major problem with this protocol was the repeated failure of the bearings in both the homogenizer and the generator.

The coarse clay was sedimented by centrifuging for one hour at 2000 rpm using an IEC model K centrifuge, at an adjusted pH of 10. Fine and medium clay was further separated using a Sharples supercentrifuge operating at 50,000 rpm, with a sample flow rate of 212 ml per minute (Tanner and Jackson, 1947). The separation of clay and silt size mica was confounded by particle shape effects; consequently, the separates were run through the supercentrifuge twice. Transmission electron microscopy was used to assess the effectiveness of the sepa-

ration. Clay separates contained very minor amounts of larger particles from the next larger particle size.

Electron probe microanalysis

Electron microanalysis was performed on the clay separates and the original mica sheet material used to make the clay. The sheet material was used as a reference material, in addition to known laboratory standards. Sheets of muscovite and biotite were carefully split into small folia and attached to petrographic slides with double sided tape. The slide mounts were carbon coated in a vacuum evaporator to prevent sample charging. Two sheets of each mica were analyzed with 30 data points per transect, on each sheet. Points of analysis were spaced apart on the specimens to prevent overlap of the analytical volumes.

Clay separates were analyzed as bulk specimens. The samples were NH_4NO_3 saturated and washed free of excess salts as determined by repeated washings with distilled deionized water (18 ohm) and the use of a Radiometer conductivity meter. Several washes with the deionized water was required to bring the conductivity near that of the background of the deionized water (5.3-5.6 μS). These saturated, salt free clays were sedimented under suction on membrane filters (0.22μm). The sedimented particles formed filter cakes of clay approximately 1.5 mm thick. The clay filtrates were transferred onto petrographic slides and carbon coated by vacuum evaporation. The clays were analyzed by moving the electron beam on a transect across the surface of the clays, obtaining 50 data points per clay mount. Points of analysis were spaced apart on the specimens to prevent overlap of the analytical volumes.

Microanalysis of the mica samples was performed on an ARL SEMQ electron microprobe, with six fixed spectrometers, three variable spectrometers, and a Kevex solid state detector.

Standards, whose composition was corroborated by dissolution analysis, were analyzed and used to optimize spectrometer alignment. A total of eighteen elements were analyzed, the sequence of analyses was set to minimize the amount of driving of the variable spectrometers. The instrument was operated at an accelerating potential of 15kV, with 200 nA emission current, and a filament (tungsten) voltage of 595 volts. Data was collected on a Digital Equipment Company PDP 11/34 computer. X-ray emission data was converted to weight percent oxide using the alpha correction factor of Ziebold and Ogilvie (1964) as amended by Bence and Albee (1968), and Albee and Ray (1970). The computer program SUPERRECAL was used to convert the weight percent oxide data into stoichiometric formulas for muscovite and biotite.

Transmission electron microscopy

Particle size distribution, morphology and basal thickness of the muscovite clays were determined on a JEOL 100C transmission electron microscope. The microscope was operated at an accelerating potential of 80 kV. A diluted aliquot of each clay separate had added to it a small amount of 0.085 μm latex spheres (E. Fullam Co.), and this suspension was evaporated on plastic-coated copper grids. The samples were coated with Pt by vacuum evaporation, enhancing morphologic features and allowing the calculation of particle thickness. The basal thickness of the mica particles was determined by comparing the length of the Pt shadows of the micas to the shadows of the latex spheres. Using the known sphere diameter, the known angle of Pt evaporation, and the shadow length, the precise heigths were calculated using the relationship: height = (shadow length)(tangent of evaporation angle).

X-ray diffraction

Clay separates of biotite and muscovite were dispersed in distilled water, adjusted to pH 8.5 with $NaCO_3$. The dispersed clays were sedimented onto porous ceramic tiles using a suction

apparatus (Rich and Barnhisel, 1977). Clays were saturated on the tiles by repeated washings with KCl or $MgCl_2$, and washed free of excess salts. After removal of excess salt, the $MgCl_2$ saturated clay was glycerol-solvated to detect the presence of any expansible layers. Heat treatments were used to characterize changes in the basal spacings of the preferentially oriented clays. The KCl tile was analyzed at room temperature, 110, 300, and 550°C. The $MgCl_2$ glycerol-solvated tile was examined at room temperature and 110°C. The saturated clays were analyzed using a General Electric/Diano 8300AD x-ray diffractometer with Nicolet software, using CuKα radiation, a graphite crystal monochromator, a 0.2 mm soller slit, and operated at 40 kV, 20 mA. Data was collected on a Digital Equipment Company PDP 11/23 computer using step scans, with two scans for each clay fraction. One set was collected from two to thirty-two degrees 2Θ (0.075 degree step width for 8 seconds), the second set was collected from six to ten degrees 2Θ (0.02 degree step width and variable count times). The step time was chosen so as to provide 25,000 counts per step. Unfortuneately, the computer software only allowed a maximum count time of four minutes. Some scans did not reach the targeted 25,000 counts, but still took thirteen hours to complete.

Thermogravimetric analysis

Thermal analyses were performed using a DuPont 1090 Thermal Analyzer, which controlled the model 901 Thermogravimetric furnace. A 10 to 15 mg aliquot of clay from the KCl saturated tiles was dryed at 110°C for four hours, prior to analysis. The dried clay was mortar and pestled to reduce inhomogeneity and then placed in the Pt sample pan in the furnace. The furnace was purged with nitrogen during data collection. Prior to initiation of the thermal runs the samples were allowed to equilibrate under the nitrogen atmosphere for at least 15 minutes, to remove as much adsorbed moisture as possible. Samples were heated from 50 to

1100°C at 20°C per minute, and weight loss recorded. Weight loss by dehydroxylation was used to quantify the water content of the clays, and this value compared to that calculated by the electron microprobe.

Surface area analysis

Specific surface area analysis of the mica clays was performed on a Micromeretics 2100D surface area analyzer. Samples were NH_4NO_3-saturated and washed free of excess salts as previously described. Samples were dessicated under vacuum at room temperature prior to analysis. Sample degassing was carried out at 50C for approximately two days. Surface areas were determined using prepurified compressed nitrogen at liquid nitrogen temperatures, and the instrument was operated as per the manufacturers instruction manual (Micromeretics Instrument Corp. Model 2100D Orr surface area analyzer). Determination of surface areas was obtained using monolayer coverage of adsorbed nitrogen (16.2 $Å^2$/molecule) and the mathematical treatment of Brunauer, Emmett and Teller (1938).

Measurement of Ion Exchange

The measurement of exchangeable cations and anions was performed according to a modified method of Laverdiere and Weaver (1977). The three clay separates of fine, medium and coarse particle size were saturated with 5 washes with 1N NaCl. The clays were then saturated by five washes at three dilute NaCl concentrations (0.001N, 0.01N, 0.1N). The 0.001N sample would usually disperse by the third washing, consequently great care was needed to avoid sample loss. Saturated clays were dried at room temperature in a dessicator under vacuum. Clay separates were mortar and pestled, and weighed into 100 ml (PMP) centrifuge tubes.

The amount of clay used in each treatment and the number of replicates was dependent on the available quantity of clay. Coarse clay particles were the most easily prepared, allowing one gram sample sizes for the eight replicates per ionic strength. Medium clay was the second most abundant which allowed the use of 500 mg samples, and up to seven replicates. There was only enough fine clay as to provide for 250 mg sample size and a reduced number of replicates. The volume of reactant solutions used was proportioned to the weight of the clay, for each clay separate. The reactant solution volume for the clays were; 20 mls for coarse clay, 10 mls for medium clay, and 5 mls for the fine clay, thus maintaining a constant clay to solute ratio. Reactant solutions were prepared containing NaCl of the three ionic strengths used to saturate the clays and containing varying milliequivalents (meq) of H^+ (as HCl). Preliminary titrations of clay separates never attained equilibrium; however, they provided estimates of the meq H^+ needed to obtain the desired ranges in pH. The combined salt and acid solution was added to the centrifuge tubes containing the clay, and shaken on a table shaker for 10 minutes. The suspensions were centrifuged for 15 minutes at 2000 rpm in an IEC (model K) centrifuge, with a swinging bucket rotor. The supernatant was saved for analysis of cations (K, Na, Al), proton activity, and the index anion Cl^-. The occluded volume in the clay was determined gravimetrically, with volumes corrected for ionic strength effects. The occluded solution was assumed to be in equilibrium with the supernatant. The clay was then washed with three volumes of 0.5N NH_4NO_3. These supernatants were analyzed for the same cations, Cl^-, and proton activity. Cation concentrations were determined by inductively coupled argon plasma spectroscopy (ICAP). Hydrogen activity in the solutions was measured with a Radiometer pH meter and a glass electrode, with a calomel reference electrode. Chloride was determined by ion specific electrode (Orion 96-17-00) using an Orion 701 ionanlyzer, and quantified by measurement from calibration curve of standards. Proton activities were .corrected using the extended Debye-Huckel calculated acitivity coefficients. Measured cation and anion exchange capacities were corrected for the occluded solution concentrations.

Chapter IV

Results

Electron probe microanalysis

Analysis of the fine clay separates of muscovite and biotite yielded analytical sums of approximately 95% (wt.) oxides, including calculated water. Analytical sums for the medium and coarse clays were nearly the same as those obtained from the sheet materials, ranging from 99 to 102% (wt.) oxides, including calculated water. Average compositions for the clays (n = 50) and sheets (n = 60) are expressed as weight percent oxides for muscovite and biotite in Table 1 and Table 2, respectively. Stoichiometric allocation of the muscovite and biotite compositions is presented in Table 3, as half-cell formulas. Water contents for muscovite (as OH) and biotite (as H_2O) were calculated as charge balancing components by SuperRecal. Comparison of water contents calculated by SuperRecal and those measured by TGA are presented in Table 4. If complementary water is added to the fine clays for a 100% analytical sum the calculated water content by EPMA approximates that by TGA.

Table 1. Weight percent oxides of muscovite clays and sheets determined by electron probe microanalysis (with H_2O calculated).

	fine clay	medium clay	coarse clay	sheet 1	sheet 2
SiO2	46.49 [a]	48.37 [b]	47.51 [c]	46.70 [a]	46.54 [a]
Al2O3	34.34 [a]	35.85 [b]	35.91 [b]	34.10 [c]	34.14 [c]
TiO2	0.13 [a]	0.14 [b]	0.14 [b]	0.16 [c]	0.16 [c]
FeO	3.01 [a]	3.06 [b]	3.10 [c]	2.51 [d]	2.53 [e]
MnO	0.10 [a]	0.12 [b]	0.12 [b]	0.07 [c]	0.07 [c]
MgO	0.27 [a]	0.32 [b]	0.35 [c]	0.27 [a]	0.27 [a]
CaO	0.04 [a]	0.07 [b]	0.05 [c]	0.02 [d]	0.02 [d]
Na2O	0.33 [a]	0.45 [b]	0.44 [b]	0.68 [d]	0.71 [d]
K2O	5.31 [a]	7.18 [b]	7.02 [c]	10.08 [d]	9.99 [e]
BaO *	(0.01)	0.00	0.00	0.00	(0.01)
Cl *	0.00	0.01	0.01	(0.01)	(0.01)
F	0.63 [a]	0.86	0.85 [b]	0.56 [c]	0.53 [c]
H2O	4.08	4.18	4.14	4.19	4.20
Sum	94.72	100.61	99.64	99.33	99.14
−O= F+Cl	0.27	0.36	0.36	0.23	0.22
SUM	94.45	100.25	99.28	99.10	98.92

Table 2. Weight percent oxides of biotite clays and sheets determined by electron probe microanalysis (with H_2O calculated).

	fine clay	medium clay	coarse clay	sheet 1	sheet 2
SIO2	38.49 [a]	40.44 [b]	39.86 [c]	40.32 [d]	40.34 [d]
Al2O3	11.35 [a]	11.43 [a]	11.24 [b]	11.43 [a]	11.19 [c]
TIO2	2.27 [a]	2.20 [b]	2.19 [b]	2.18 [b]	1.98 [c]
FeO	19.66 [a]	19.02 [b]	18.79 [c]	17.98 [d]	17.79 [e]
MnO	0.99 [a]	0.98 [a]	1.00 [b]	0.98 [a]	0.98 [a]
MgO	12.84 [a]	14.30 [b]	14.64 [c]	14.56 [c]	14.46 [c]
CaO	0.06 [a]	0.06 [b]	0.06 [b]	0.05 [c]	0.05 [c]
Na2O	0.28 [a]	0.33 [b]	0.44 [c]	0.52 [d]	0.51 [d]
K2O	4.77 [a]	7.08 [b]	8.64 [c]	9.14 [d]	9.19 [e]
BaO *	0.09 [a]	0.12 [b]	0.14 [c]	0.14 [c]	0.15 [c]
Cl *	0.07 [a]	0.06 [b]	0.07 [b]	0.06 [b]	0.06 [b]
F	2.87 [a]	3.31 [b]	3.40 [c]	3.71 [d]	3.58 [e]
H2O	2.49	2.49	2.44	2.33	2.36
Sum	96.23	101.82	102.91	103.40	102.64
−O= F+Cl	1.22	1.41	1.45	1.58	1.52
SUM	95.00	100.41	101.46	101.82	101.12

Table 3. Stoichiometric half-cell formulas of muscovite and biotite (clays and sheets) allocated by SuperRecal.

MUSCOVITE

Fine Clay	$K_{0.46}Na_{0.04}[Al_{1.92}Fe_{0.17}Mg_{0.03}]^{VI}[Si_{3.16}Al_{0.84}]^{IV}O_{10}(OH)_{1.86}F_{0.13}$
Medium Clay	$K_{0.59}Na_{0.05}[Al_{1.86}Fe_{0.16}Mg_{0.03}]^{VI}[Si_{3.13}Al_{0.87}]^{IV}O_{10}(OH)_{1.82}F_{0.18}$
Coarse Clay	$K_{0.59}Na_{0.05}[Al_{1.87}Fe_{0.17}Mg_{0.03}]^{VI}[Si_{3.11}Al_{0.89}]^{IV}O_{10}(OH)_{1.82}F_{0.18}$
Sheet 1	$K_{0.86}Na_{0.09}[Al_{1.81}Fe_{0.14}Mg_{0.03}]^{VI}[Si_{3.12}Al_{0.87}]^{IV}O_{10}(OH)_{1.88}F_{0.12}$
Sheet 2	$K_{0.85}Na_{0.09}[Al_{1.81}Fe_{0.14}Mg_{0.03}]^{VI}[Si_{3.12}Al_{0.88}]^{IV}O_{10}(OH)_{1.89}F_{0.11}$

BIOTITE

Fine Clay	$K_{0.46}Na_{0.04}[Mg_{1.45}Fe_{1.25}Ti_{0.13}Mn_{0.06}]^{VI}[Si_{2.92}Al_{1.01}]^{IV}O_{10}(OH)_{1.30}F_{0.69}$
Medium Clay	$K_{0.65}Na_{0.05}[Mg_{1.54}Fe_{1.15}Ti_{0.12}Mn_{0.06}]^{VI}[Si_{2.91}Al_{0.97}]^{IV}O_{10}(OH)_{1.24}F_{0.75}$
Coarse Clay	$K_{0.79}Na_{0.06}[Mg_{1.57}Fe_{1.13}Ti_{0.12}Mn_{0.07}]^{VI}[Si_{2.87}Al_{0.95}]^{IV}O_{10}(OH)_{1.22}F_{0.77}$
Sheet 1	$K_{0.83}Na_{0.07}[Mg_{1.55}Fe_{1.07}Ti_{0.17}Mn_{0.06}]^{VI}[Si_{2.88}Al_{0.96}]^{IV}O_{10}(OH)_{1.16}F_{0.84}$
Sheet 2	$K_{0.84}Na_{0.07}[Mg_{1.55}Fe_{1.07}Ti_{0.11}Mn_{0.06}]^{VI}[Si_{2.90}Al_{0.95}]^{IV}O_{10}(OH)_{1.18}F_{0.81}$

Table 4. Weight percent water contents calculated by SuperRecal and measured by Thermogravimetric analyses.

Muscovite	EPMA	TGA
fine clay	4.08 %	9.22 %
medium clay	4.18	5.09
coarse clay	4.14	5.05
sheet 1	4.19	
sheet 2	4.20	

Biotite	EPMA	TGA
fine clay	2.49 %	2.52 %
medium clay	2.49	1.20
coarse clay	2.44	0.44
sheet 1	2.33	
sheet 2	2.36	

Comparison of the weight percent oxide compositions of the muscovite clays indicates a difference between the fine clay content of; K, Na, Mg, F, and H_2O and those of the medium and coarse clays. The medium and coarse muscovite clays were nearly identical in composition. The statistical significance of the differences will be discussed subsequently. Similar compositional variations exist amongst the biotite clays. The fine clay biotite contains reduced levels of Si, Mg, Na, K, F, and H_2O, relative to the medium and coarse biotite fractions. A slight increase in Fe content of the fine clay biotite, relative to the larger biotite clays and sheets, was observed. The comminution of the biotite with stainless steel knife blades may have contributed to the Fe content of this clay size. Finely abraded particles of the steel blades may occur as colloidal material, which may have been inadvertently added to the sample. However, there was no increase in the Fe content of the fine clay muscovite, nor was there evidence of steel particles or fragments in either of the fine clays when examined by TEM.

Stoichiometric allocation of the oxide data by SuperRecal partitioned elements according to theoretical constraints on the mica structures, for muscovite and biotite. Silicon, in muscovite, was allocated into tetrahedral coordination with the remaining tetrahedral sites filled with Al. The additional Al was then partitioned into octaheral coordination, with the cations; Ti, Fe, Mn, and Mg. For biotite, all of the Al and Si were allocated to tetrahedral positions. There was no extra Al to be added to the octahedral cations. SuperRecal assigned the divalent Ca and Ba ions and monovalent Na and K, to satisfy interlayer charge. Stoichiometric allocations reflect well the differences reported as weight percent oxides (Table 3). Unfortuneately, SuperRecal could not accomodate the 0.3% (wt.) of Rb in muscovite into the stoichiometric partitioning.

A significant decrease of K was observed in the fine clay fractions of both minerals. The K content of the fine muscovite (0.992 wt. %) indicates nearly a 50% reduction in interlayer charge from that found in the muscovite sheets. None of the other interlayer cations increased to compensate the change in charge; however, there was a decrease in tetrahedral Al and a corresponding increase in octahedral Al. The reduction of tetrahedral Al may signify a pref-

erential orientation of planes of weakness to cutting. The tetrahedral substitution of Al or the vacant octahedral site may provide planes susceptable to mechanical stresses during grinding. Alternatively, the decreased interlayer charge due to K removal may invoke a shift in the site of charge compensation to the octahedral Al. The slightly decreased weight percent content of water in the fine clay muscovite, and the lower analytical sum may obscure the increase in water (OH) content calculated in the fine clay stoichiometry. An increase in water content may represent a charge compensating component of the fine muscovite. Changes in the fine biotite clay were more complex with; decreased interlayer K, Na, and octahedral Mg. Corresponding increases in tetrahedral Al and in octahedral Fe and Ti were observed. The decrease in interlayer components seemingly contradicts the apparent increase in tetrahedral substitution. The increased Fe and Ti in the octahedral sheet are also enigmatic, raising questions about sample preparation and particle size and particle shape influences on EPMA analysis.

Despite interpretive uncertainties, generally the relative abundances of all elements were consistent between the mica sheet material and the clays. Of the eighteen elements determined Ca and Cl were of sufficiently low abundance as to be considered as background levels. Neither muscovite nor biotite (clays or sheets) contained Zn, Ba, Cr, Ni, P, nor Sr above 0.07 weight percent. Muscovite did contain noteable quantities of Rb (0.3% wt.). The Rb component could not be incorporated into the analytical scheme for SuperRecal stoichiometry. Likewise, Li was not addressed in this analytical method. Its absence may have been a source of error regarding octahedral partitioning.

Statistical analysis

Statistical analyses were performed on the weight percent oxide data to test for normality of distribution and variance, with particle size being the treatment effect. Data from the different clay sizes was assumed to be independent. Likewise, the composition of the original sheet material was assumed to be independent from the clays. The Shapiro-Wilks test for normality

($\alpha = 0.05$) and an analysis of variance ($\alpha = 0.05$) were performed. The results of these tests are indicated in Tables 1 and 2, in which superscripts denote between group differences for variance, and asterisks indicate nonnormal distribution within groups. The effects of closure were avoided because the weight percent oxides were not constrained to sum to 100% (Johansson et al., 1984), and negative values were not subtracted. Negative values were treated as being at background level for these elements.

Analysis of variances between the different clays sizes of muscovite indicate significant compositional differences exist between the fine clay and the medium and coarse clays. Statistically, the null hypothesis of no treatment (particle size) differences was rejected for comparisons between the fine clay and the larger clays. With the exception of the trace elements Zn, Ni, and Sr, none of the elements of the fine clay came from the same population as the medium and coarse clays. Differences between the medium and coarse clays were not as abundant as those with the fine clay, however, treatment effects were evident for the elements; Si, Mg, Fe, K, Ca, Zn, Ba, and Cl. The remaing elements could have come from the same population (Al, Ti, Mn, Na, F, Ni, Cr, P, Sr, and Rb). Variances between the two muscovite sheets were small, enabling acceptance of the null hypothesis regarding all elements except Fe, and K.

Variance between the biotite clays was not as consistent as for the muscovite clays. Significant differences exist between the three clay sizes, with the exception of Ni, and Sr for which no differences exist. The null hypothesis is not rejected when comparing fine and medium clay contents for the elements; Al, Zn, and Mn. Similarly, there were no differences between the fine and coarse clay contents for the trace element Cl. There was no difference between Ca, and Rb for the medium and coarse clays. Overall, the variability of the biotite clays was large. The null hypothesis, for the biotite sheets, was rejected for the elements; Al, Fe, K, F, and Ti. The variability of the initial biotite sheets was large, which may account for some of the clay variability.

Transmission electron microscopy

The clay fractions of both muscovite and biotite possess similar particle morphologies. The fine clay fractions of both minerals contain abundant lath shaped particles (Figure 1). The lath shaped particles lend credence to the proposal that soil hydrous mica is small particle size muscovite, with decreased K and increased hydration. The isolation and mineralogical characterization of the 10Å soil component is needed to substantiate such conjecture. The medium and coarse fractions of biotite and muscovite were primarily composed of angular and fan shaped particles (Figs. 2, 3, respectively), which were typical for these micas (Beutelspacher and van der Marel, 1968). However, the fan shaped particles exhibited the bending of 2:1 layers by the shearing of the cutting blades, during particle grinding. The hardness of micas differ significantly dependent on the surface tested (Switzer, 1941), orientation of the test and composition (Bloss, 1959). Production of clays was effected by combined delamination of 2:1 layers and shearing, normal to the basal surfaces. It was the shearing normal to basal surfaces that produced the fan morpholgies. The abundance of fan shaped particles in the fine clay muscovite suggests that the dioctahedral mineral was less susceptible to stripping of the tetrahedral layers, than biotite clays. Analysis of selected area diffraction (SAD) patterns for the clays does not indicate a difference in layer stacking sequence or crystallinity, due to comminution. The SAD micrographs were taken when resolution and intensity of diffraction were optimized, however, this does not mean that crystal orientation was ideal. A preferred SAD orientation was not obtainable for the clay particles; therefore, its use here is intended only to establish crystallinity of the clays. Composite plots of particle height distributions versus the number of observations at a particular height (frequency) are presented for the fine clays (Figure 4), medium clays (Figure 5), and coarse clays (Figure 6) of biotite and muscovite. Basal areas were also measured, and their distributions plotted as composites for the fine clays (Figure 7), medium clays (Figure 8), and the coarse clays (Figure 9).

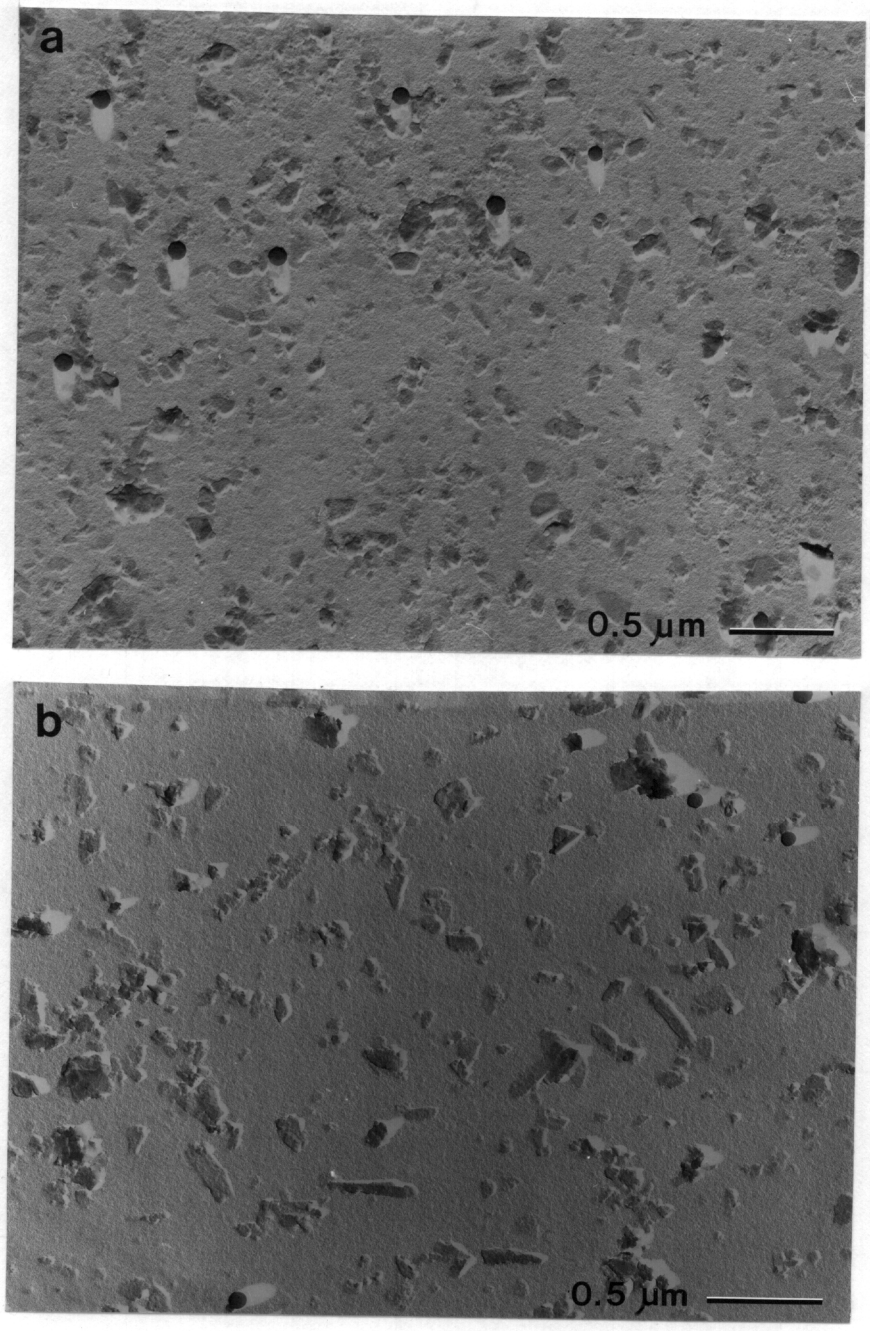

Figure 1. Transmission electron micrographs of the fine clay (0.08 µm) fractions of a) biotite and b) muscovite.

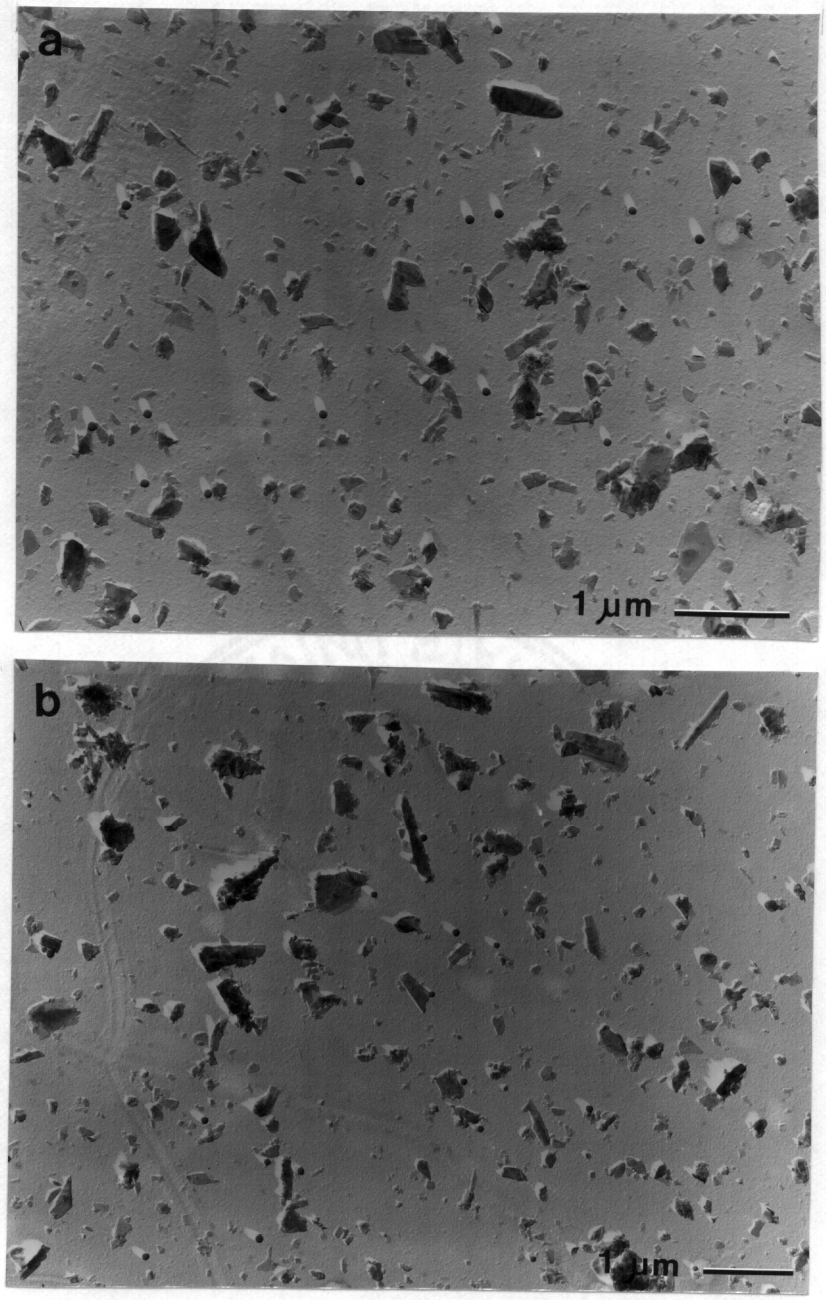

Figure 2. Transmission electron micrographs of the medium clay (0.08-0.2 µm) fractions of a) biotite and b) muscovite.

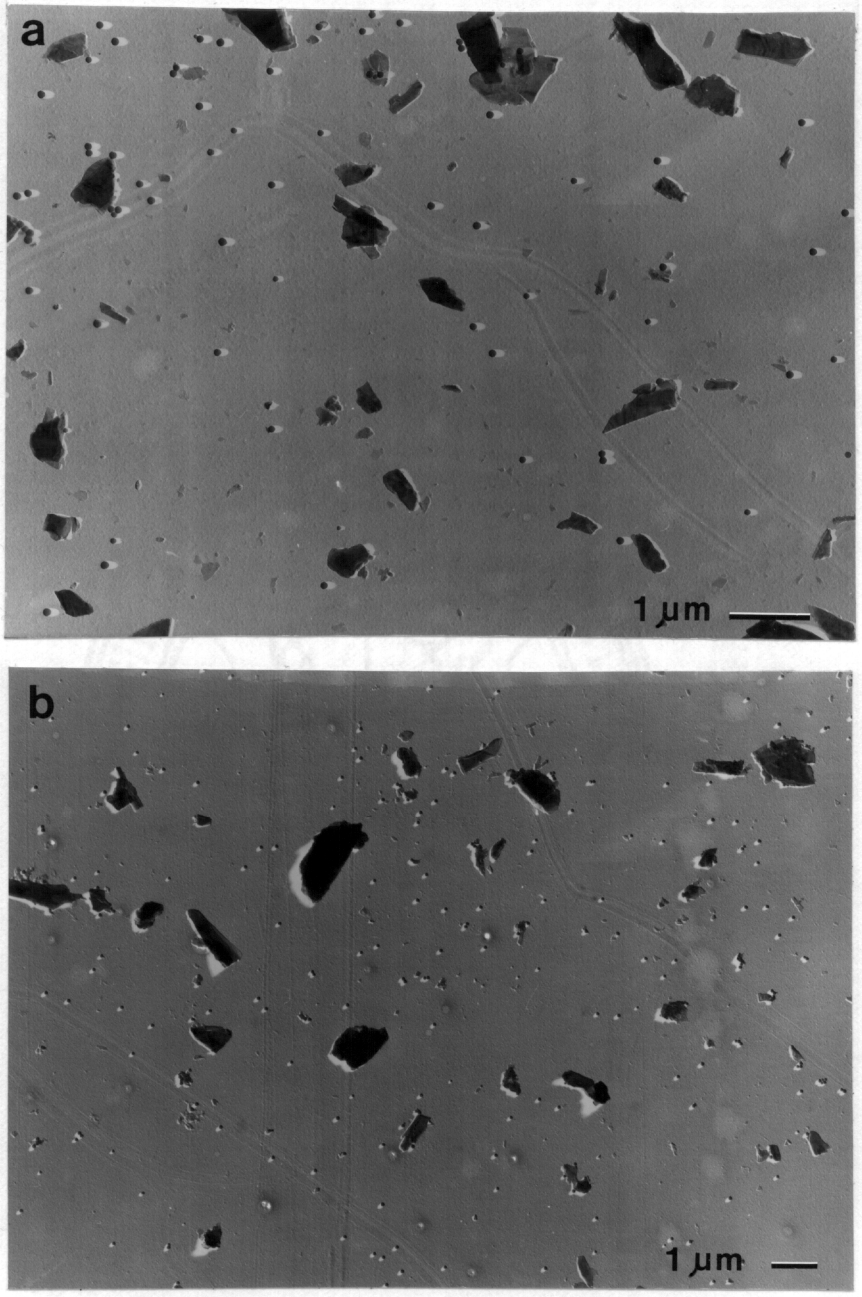

Figure 3. Transmission electron micrographs of the coarse clays (0.2-2.0 µm) fractions of a) biotite and b) muscovite.

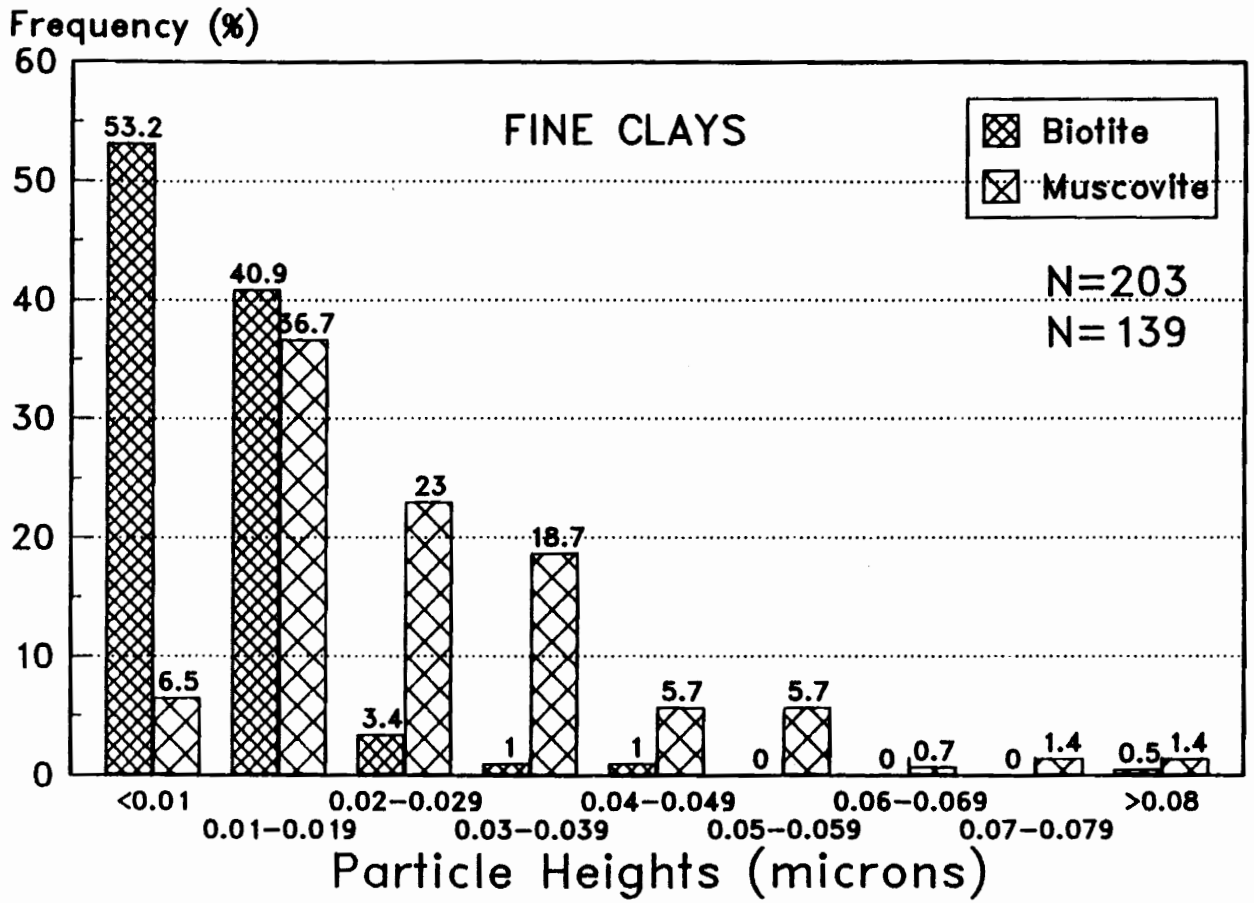

Figure 4. Distribution of particle heights measured by electron microscopy for the fine clays of biotite and muscovite.

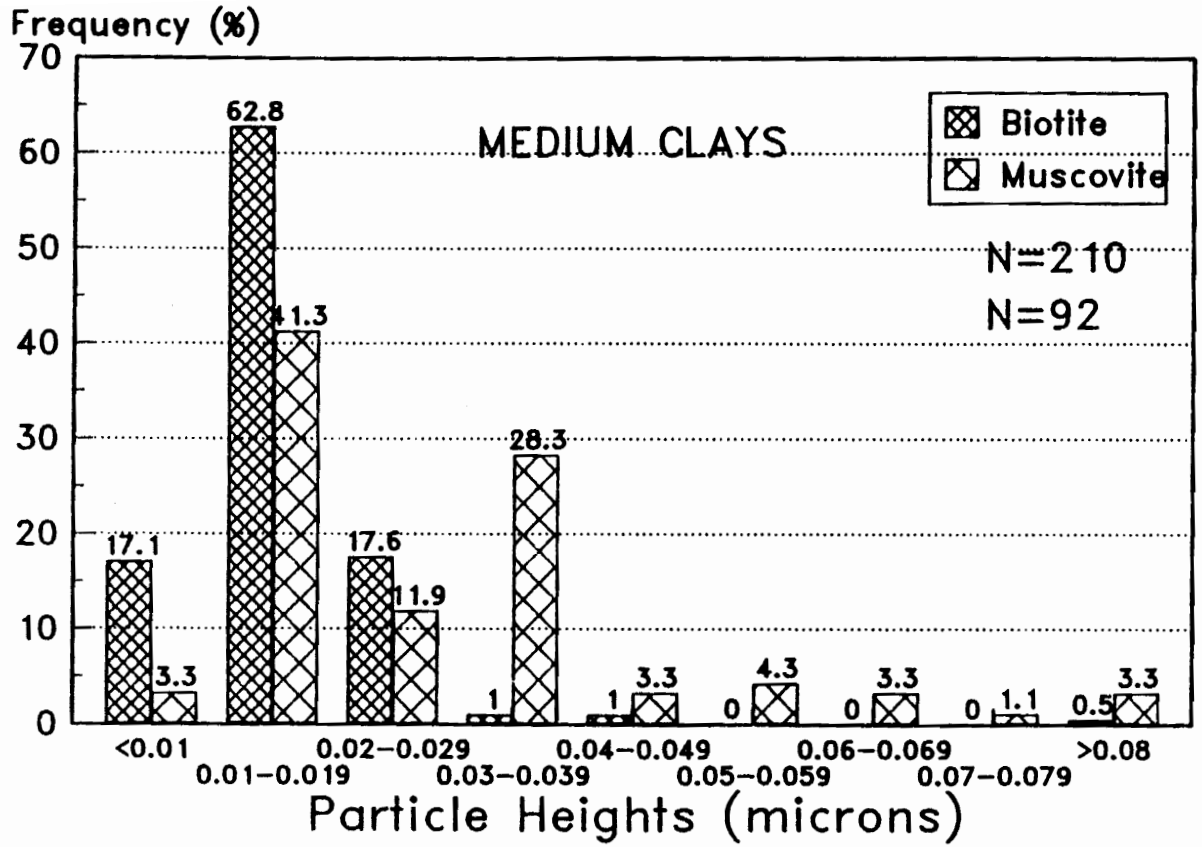

Figure 5. Distribution of particle heights measured by electron microscopy for the medium clays of biotite and muscovite.

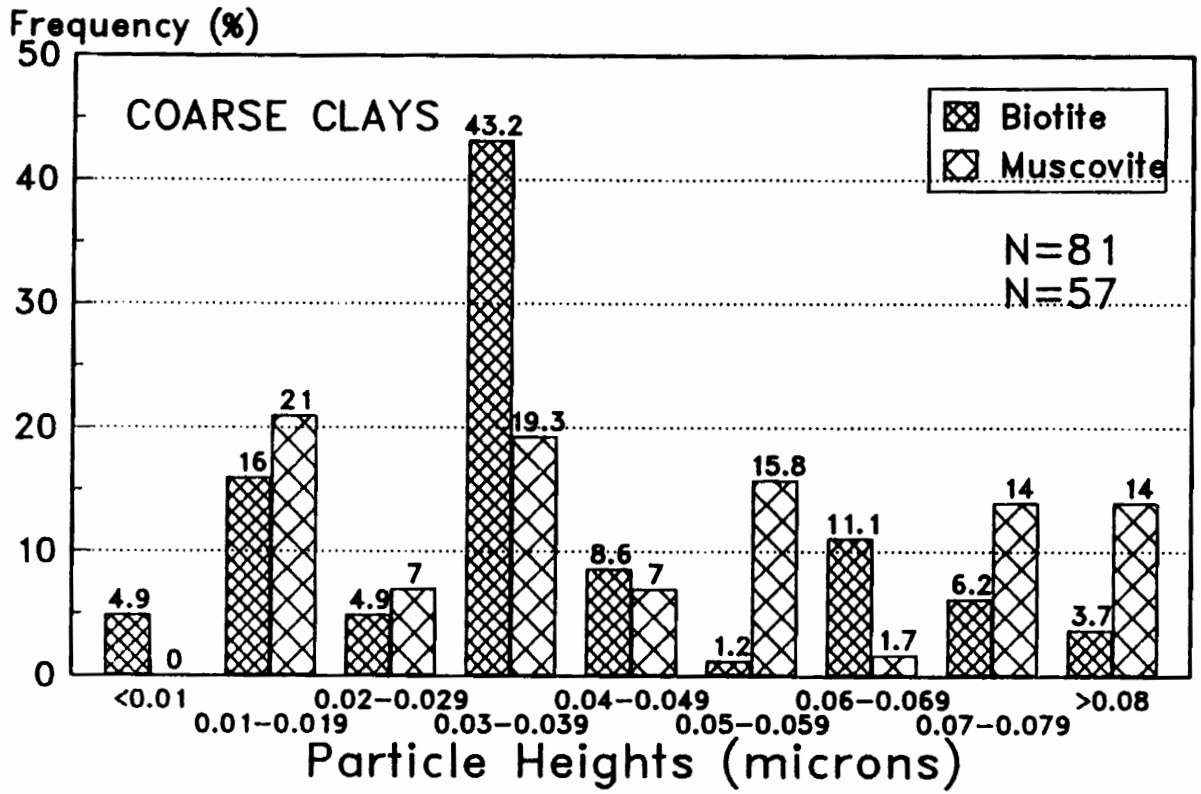

Figure 6. Distribution of particle heights measured by electron microscopy for the coarse clays of biotite and muscovite.

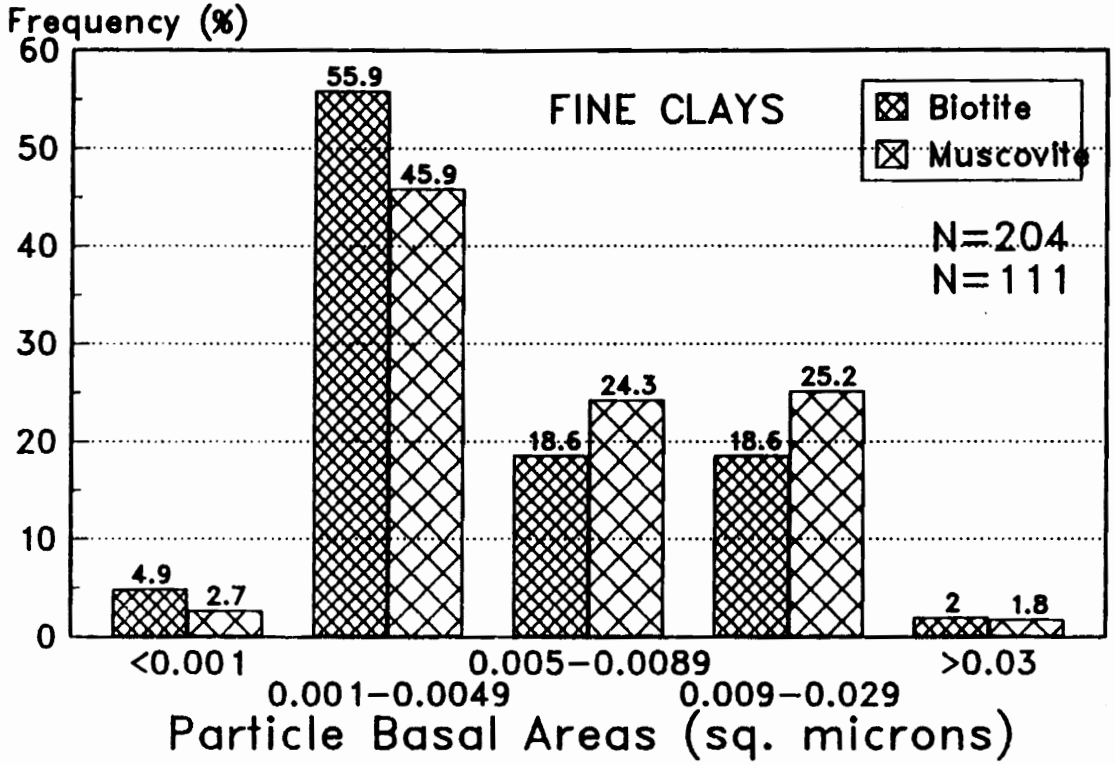

Figure 7. Distribution of basal areas measured by electron microscopy for the fine clays of biotite and muscovite.

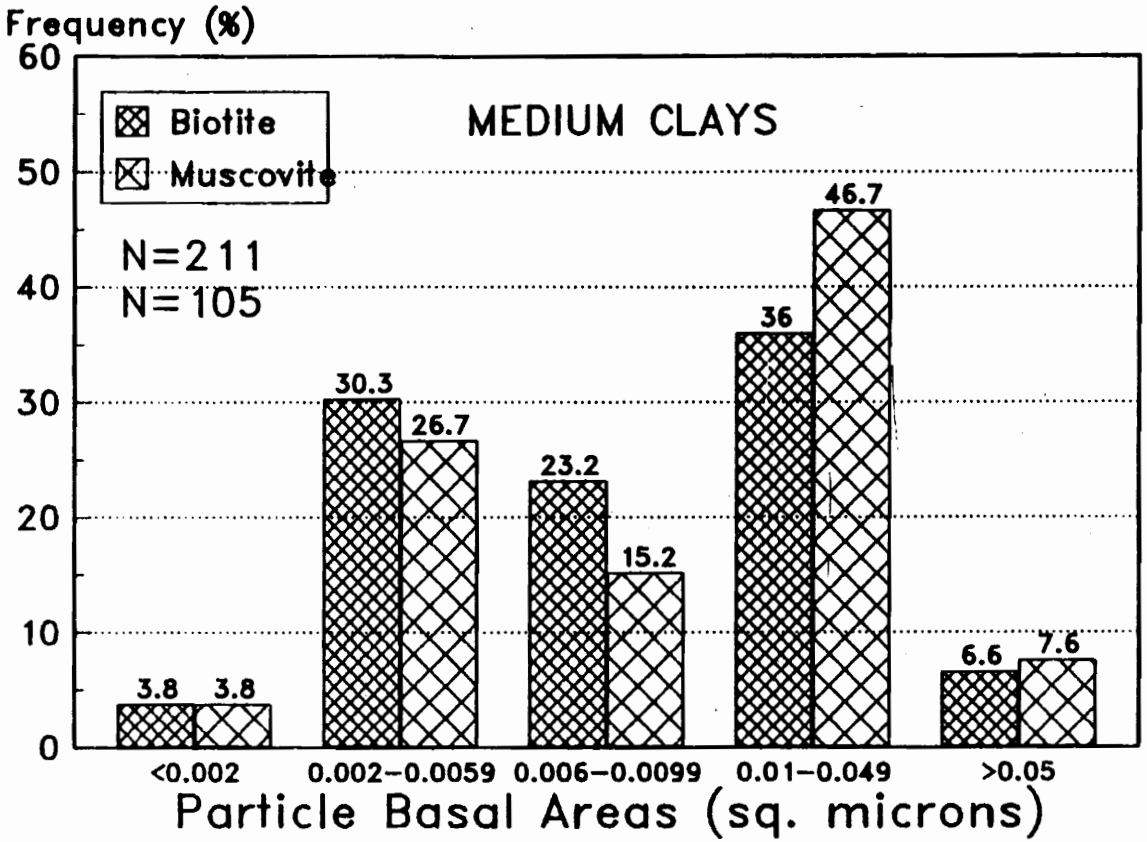

Figure 8. Distribution of basal areas measured by electron microscopy for the medium clays of biotite and muscovite.

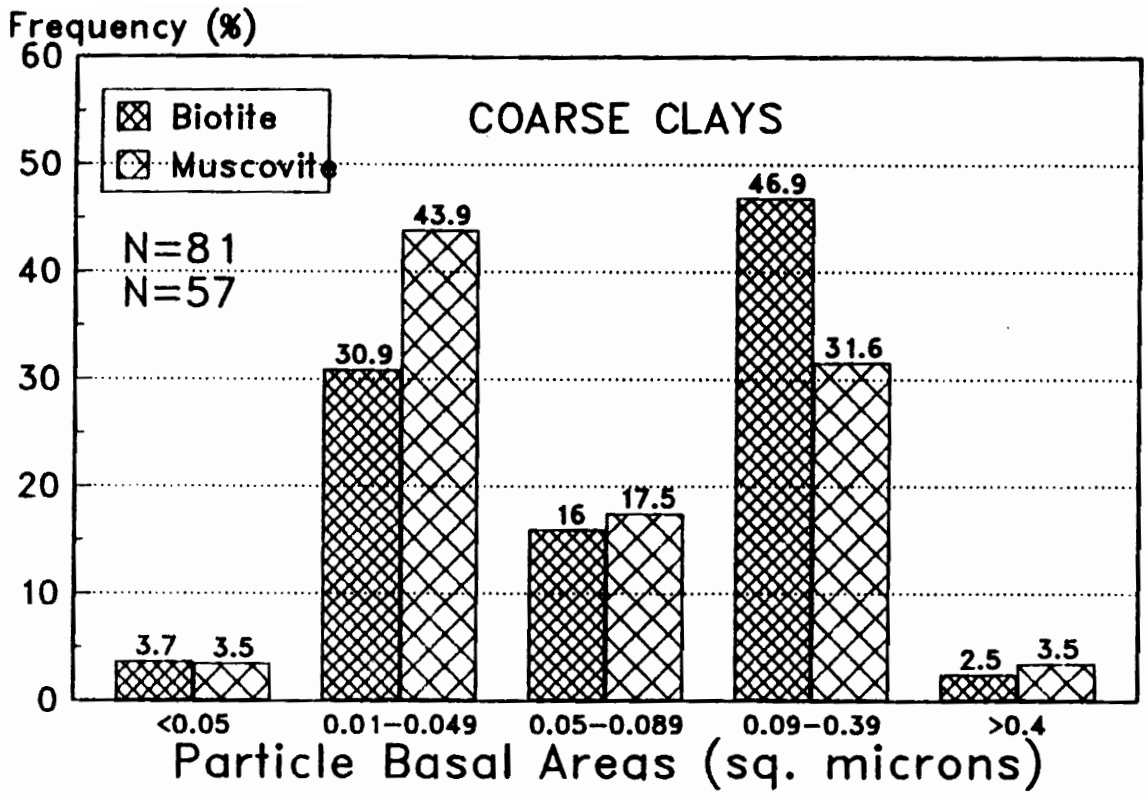

Figure 9. Distribution of basal areas measured by electron microscopy for the coarse clays of biotite and muscovite.

The distribution of particle heights for both mica clays suggests that dioctahedral muscovite is more resistant to delamination than the biotite. Particle heights for the fine clay biotite are strongly skewed to the smallest height intervals ($<0.01\mu m$ and 0.01-0.02 μm). More than 94% of the fine biotite is less than 0.02 μm thick. By comparison, only 43% of the muscovite particles have heights in this range. Most of the medium biotite particles (97.5%) have heights less than $0.03\mu m$, whereas medium muscovite only has 56.5% of its particles witin this range of heights. This evidence suggests stripping of tetrahedral layers may account for the lower particle heights of the biotite clays, however, conclusive evidence to support this proposal has not been found.

X-ray diffraction

Diffraction maxima for the clays were significantly affected by the small particle sizes. Peak broadening and decreased diffraction intensity were severe for the fine clays. Although each clay separate had two ceramic tiles prepared, one saturated with KCl and the other $MgCl_2$, only the K saturated clays will be discussed because the results from the Mg samples were virtually identical. Following is a summary of the diffraction characteristics of each clay fraction, for both micas.

The fine muscovite clay was x-rayed as a semirandom powder mount because of curling and exfoliation of the clay from the ceramic tile mount, when dry. The fine muscovite clay exhibited a very broad and weak 10Å peak (Figs. 10,11), an asymmetric second order (5.0Å) reflection, and a very broad third order peak (3.3Å). The second order peak consistently increases in intensity with heating, up to 550°C. Medium muscovite clay provided much more coherent diffraction from basal planes than the fine clay (Figure 12). Interestingly, the first, second and third order peaks increased in intensity when heated from 25 to 110°C, and then intensity decreased with further heating to 300 and 550°C. There were no basal spacing shifts associated with the changing peak intensity, however, there were weak nonbasal reflections

at all temperatures. The coarse muscovite gave strong basal reflections (Figure 13) and abundant non-basal reflections at all temperatures. The basal peak intensity increased as it did for medium clays at 110°, decreased at 300°, and then increased again slightly at 550°C (Figure 14). The non-basal reflections have been ascribed to numbers of smaller particles which did not achieve the same degree of preferential orientation during suction sedimentation on the ceramic tiles.

Fine clay biotite gave more coherent basal diffraction than fine muscovite. This was at least partly due to the muscovite being a semirandom powder mount. All three basal reflections (10Å, 5Å, 3.3Å) were asymmetric and broad (Figure 15). The occurrence of the second order reflection suggests that the fine clay was not Fe-rich (Grim, 1968). However, EPMA indicates that the fine clay contains the most Fe of the biotite clays. The second order reflection was absent from the medium and coarse biotite clays (Figs. 16,17). Heating caused a slight increase in intensity of the 10Å peak of the fine and medium clays. At 300° the 10Å peak of medium clay lost a small amount of intensity, but then intensified again at 550°C. The third order reflection also intensified with heating. Basal spacings of the medium clay were unaffected by heating. Conversely, the coarse clay underwent significant basal collapse when heated (Figure 18). Initially, the first order peak occurred at 10.2Å at 25° and at 10.1Å between 110 and 300°C. At 550°C the basal spacing was 10.0Å. The small shift between 25° and 300°C was accompanied by an increase in reflection intensity. Concomitant with the final collapse was a 31% decrease in intensity between 300 and 500°C. The structural rearrangement indicated by the partial collapse of the basal spacing may be due to the combined effect of Fe oxidation, unit cell dimensional changes, and rearrangement of the OH orientation within the ditrigonal hole.

Thermal analysis

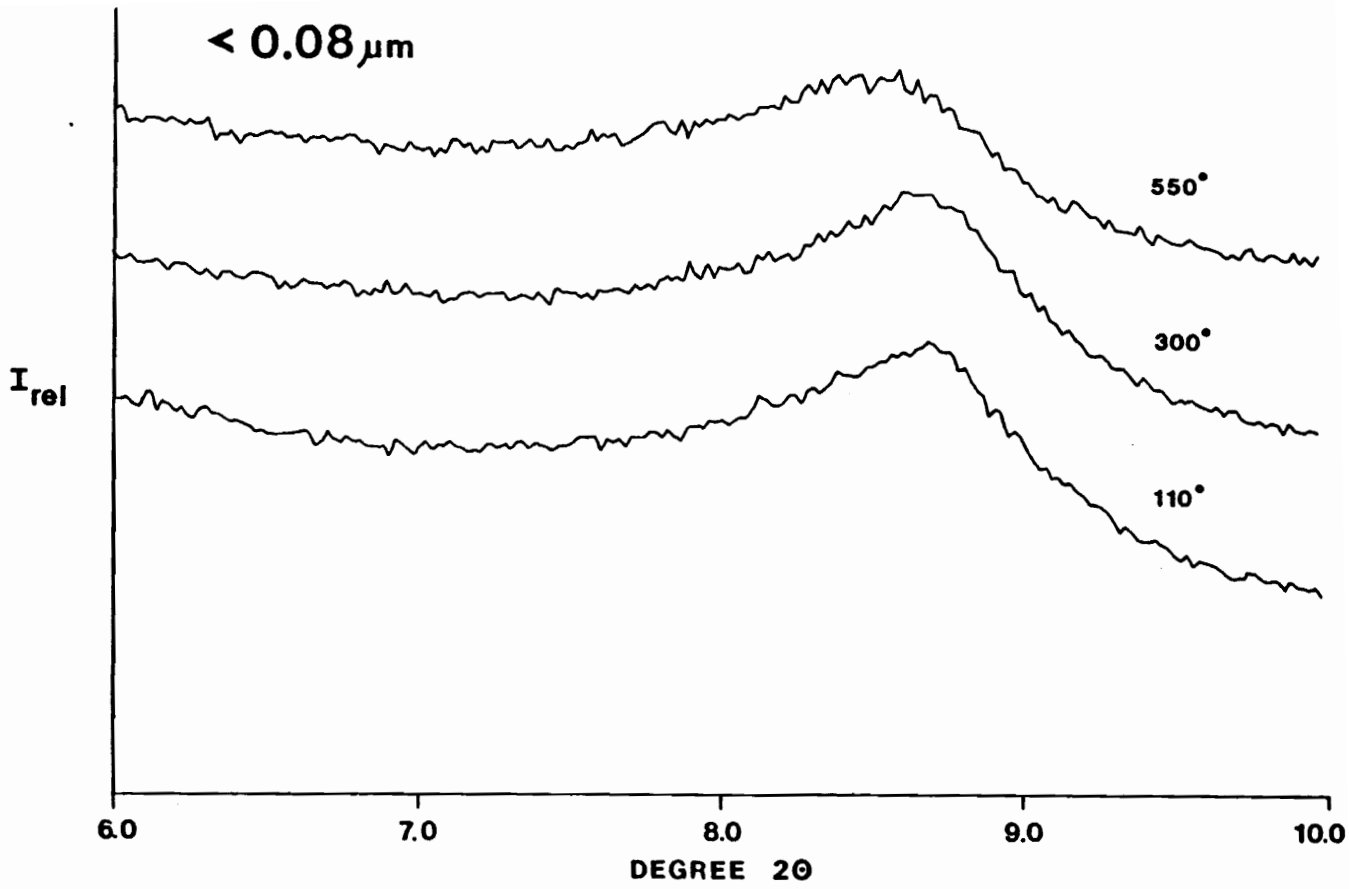

Figure 10. X-ray diffractogram of the extremely broad and weak 10Å peak of fine clay muscovite.

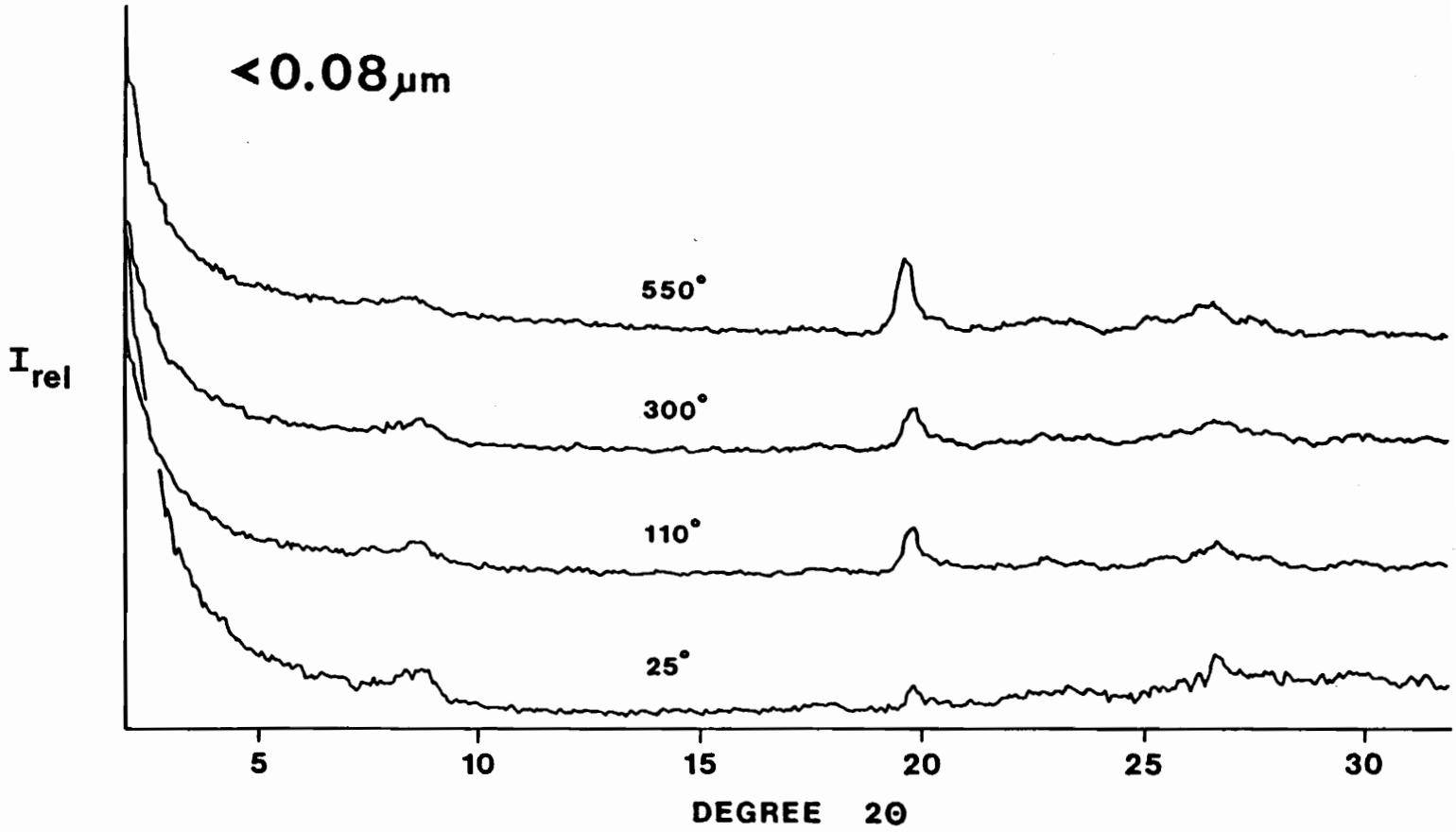

Figure 11. X-ray diffractogram of fine clay muscovite from 2 to 32 degrees 2θ, exhibiting very weak diffraction maxima.

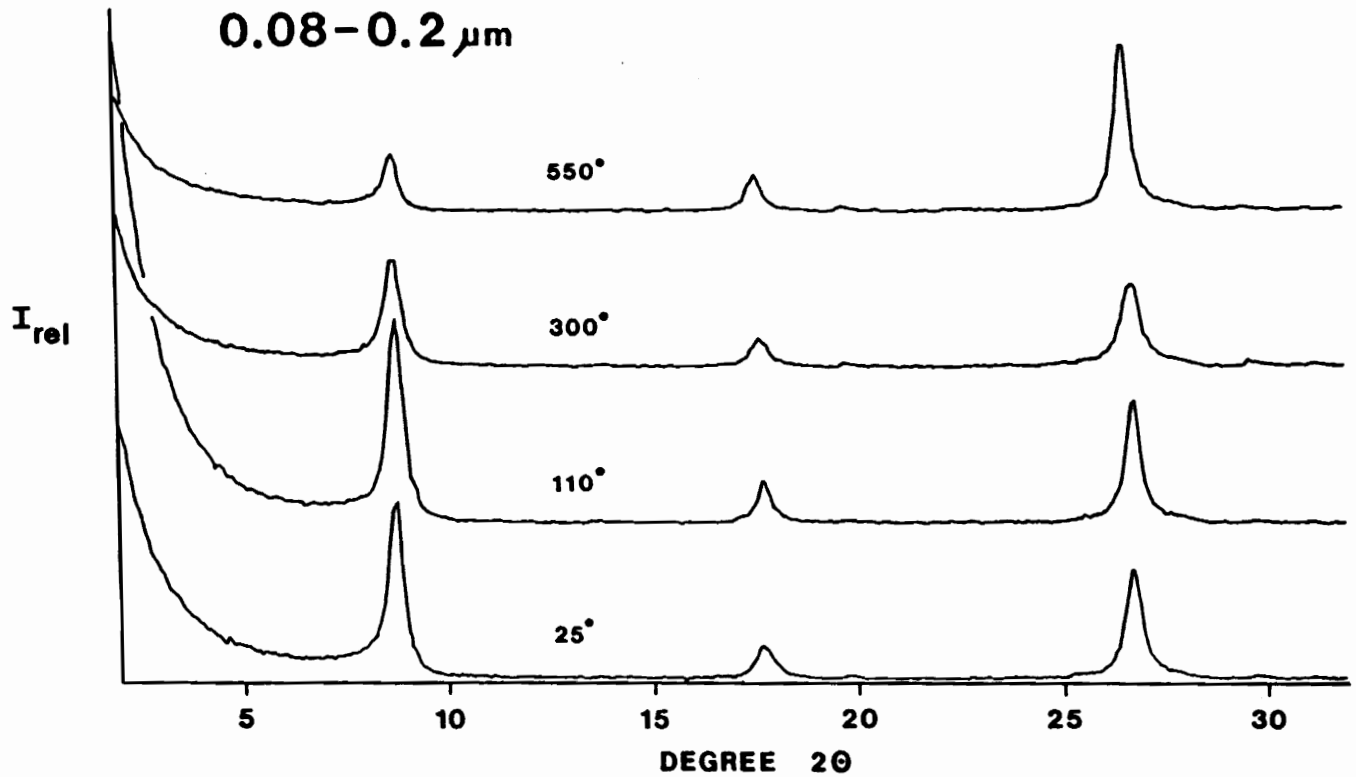

Figure 12. X-ray diffractogram of medium clay muscovite possessing weak nonbasal and strong basal reflections.

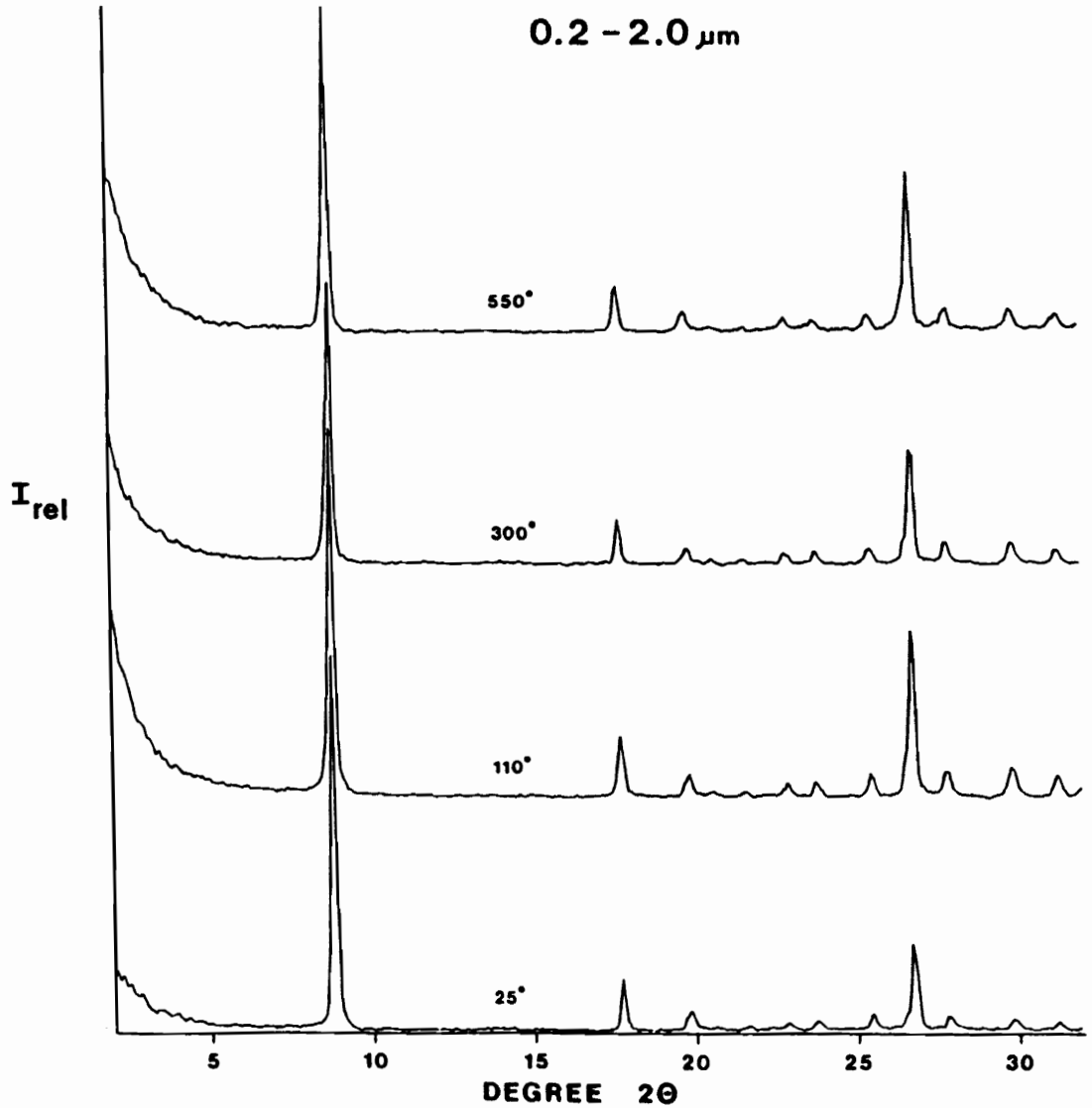

Figure 13. X-ray diffractogram of coarse clay muscovite exhibiting strong basal and nonbasal reflections at all temperatures.

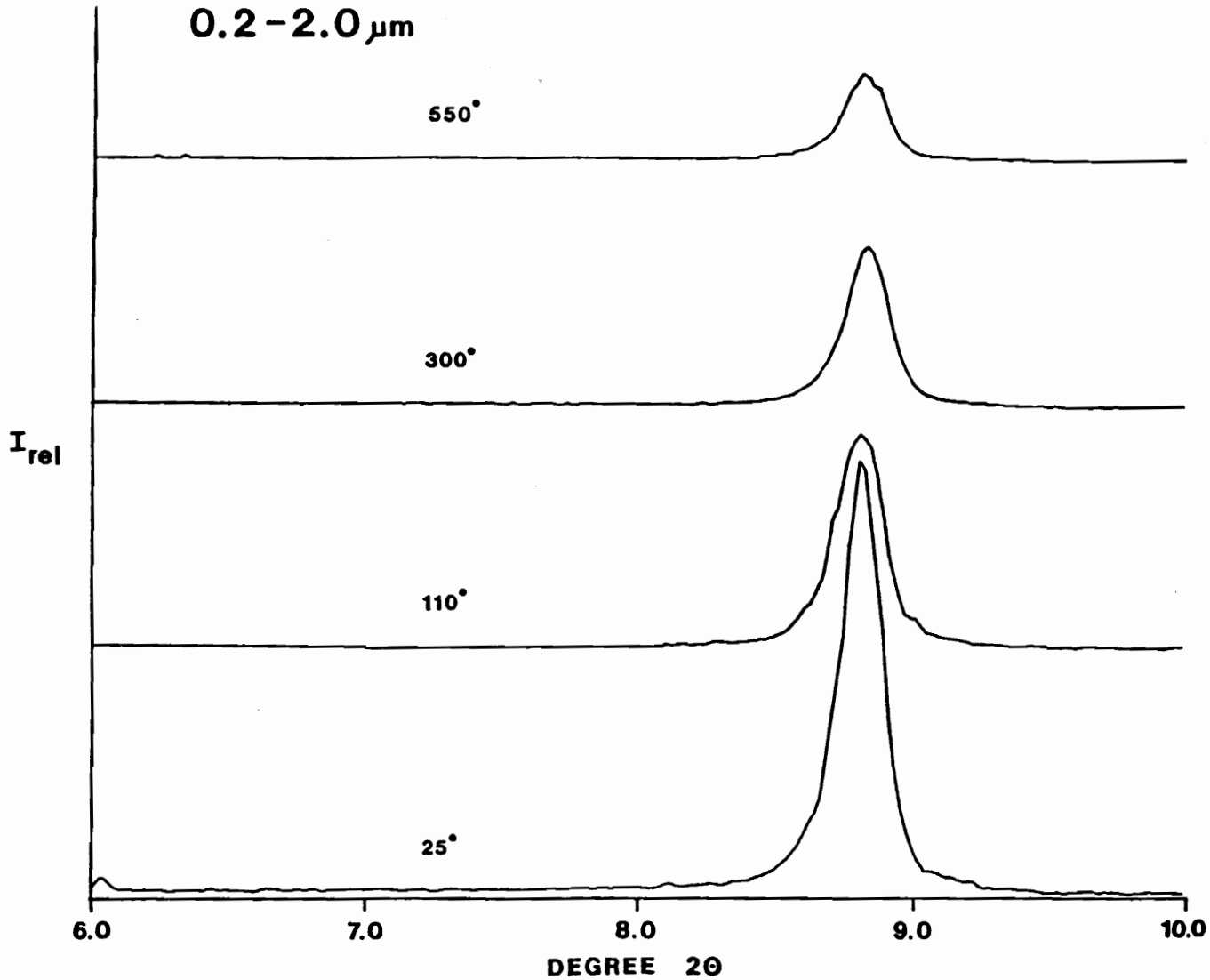

Figure 14. X-ray diffractogram of the 10Å peak of coarse muscovite displaying heat induced reduction of intensity.

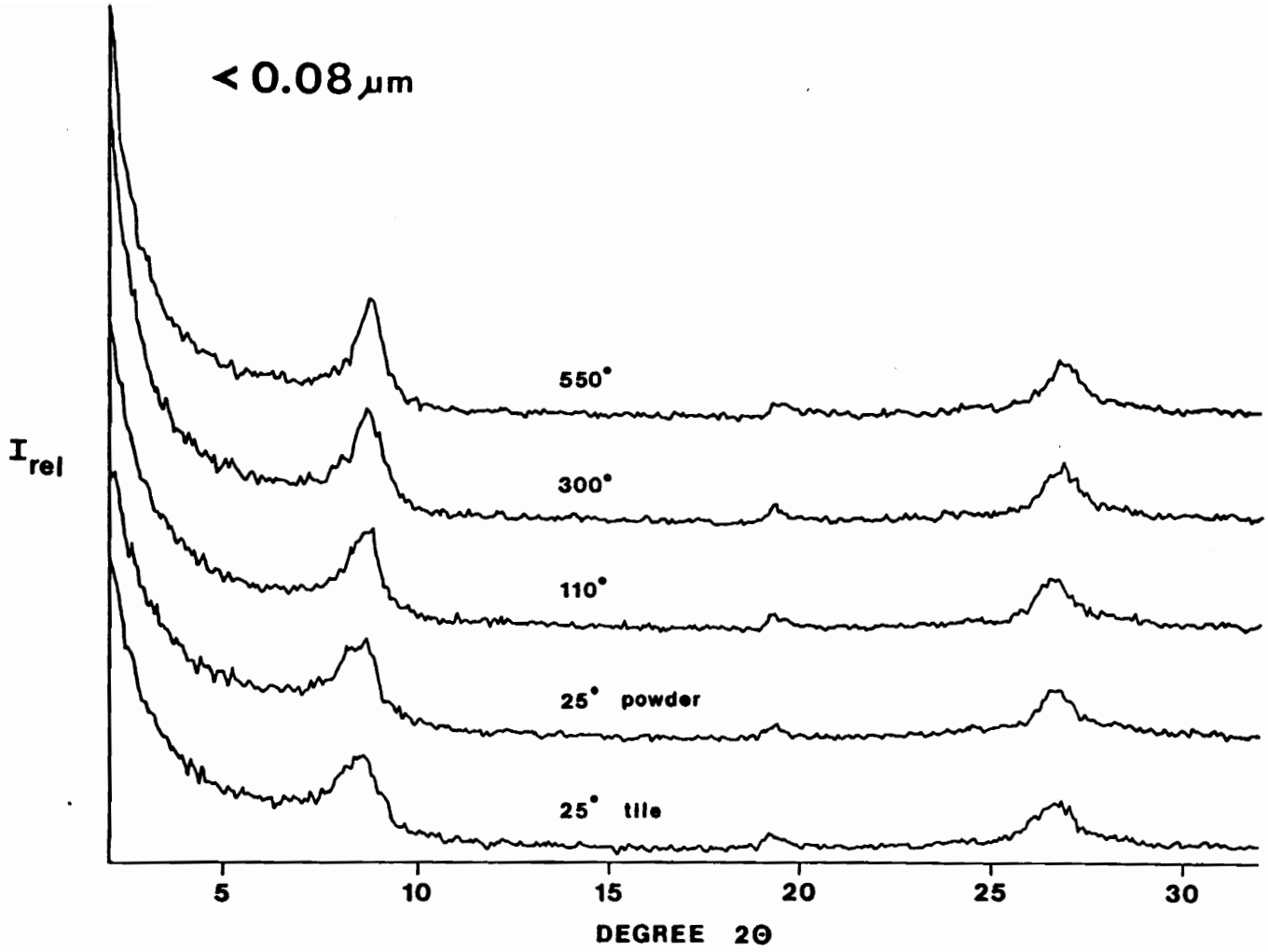

Figure 15. X-ray diffractogram of the extremely broad and weak basal reflections of fine clay biotite.

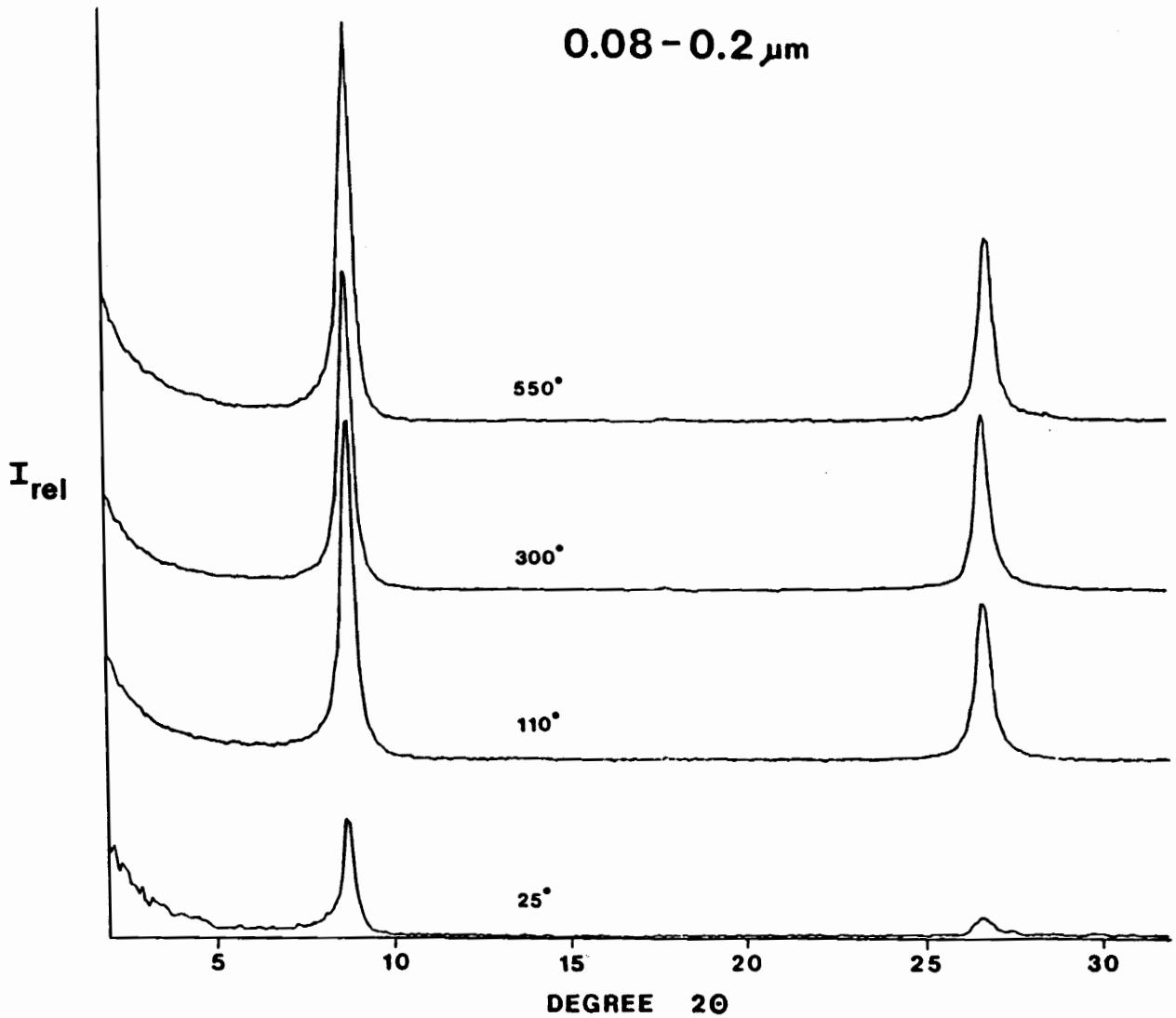

Figure 16. X-ray diffractogram of medium clay biotite exhibiting heat dependent changes in peak intensities.

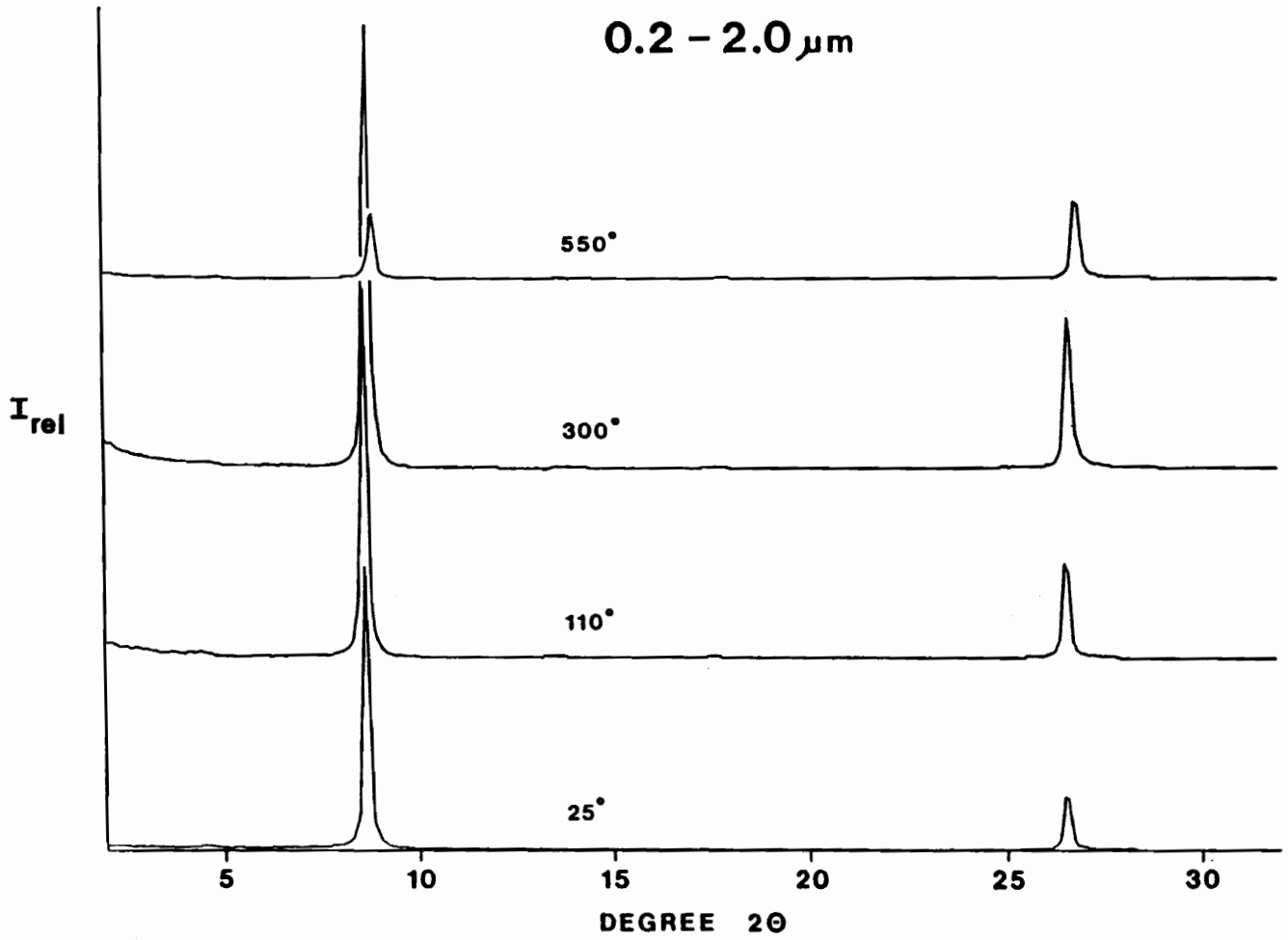

Figure 17. X-ray diffractogram of coarse clay biotite exhibiting heat dependent changes in peak intensities.

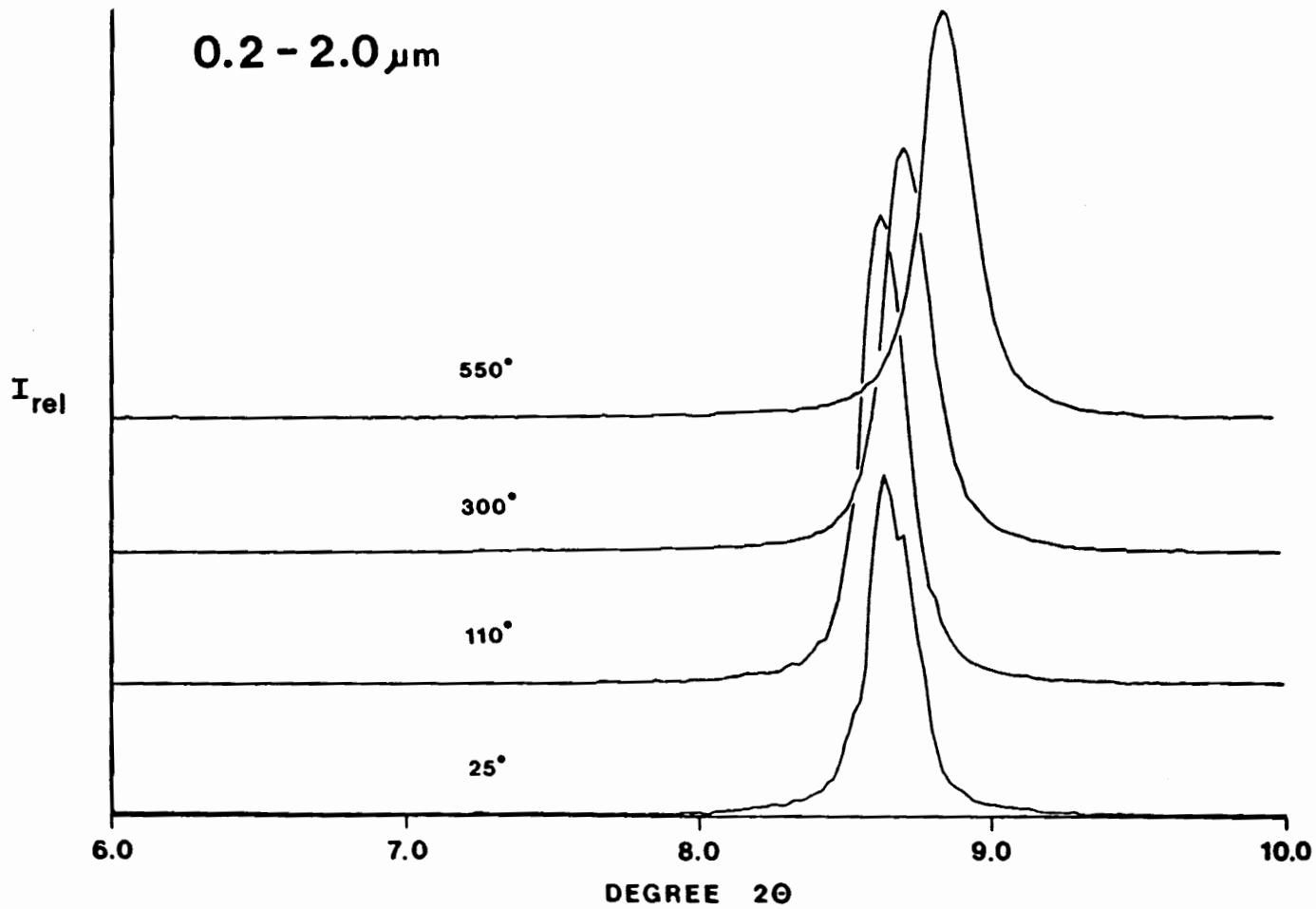

Figure 18. X-ray diffractogram of the 10Å peak of coarse clay biotite displaying the collapse of basal spacing with heating.

The observed thermogravimetric data for the mica clays was consistent with accepted behavior of macroscopic mica specimens. The only apparent difference between the thermal behavior of the clays and macroscopic specimens was the temperatures of dehydration and dehydroxylation for the clays were significantly lower (100-300° lower). All fractions of the biotite and muscovite clays exhibited typical low temperature (<150°C) weight loss of adsorbed atmospheric moisture. The initial rapid weight loss was largest in the fine clay, then correspondingly smaller loses by the medium and coarse clays. Adsorbed atmospheric mositure is primarily a function of the external surface areas of the clays. Finer particles present proportionally more area for the coordination of adsorbed phases. The larger external surfaces also provide more area from which dehydration may occur, at higher temperatures.

Between approximately 150 and 550°C the clays lost weight due to dehydroxylation of the crystal structure. The distinction between removal of adsorbed atmospheric water and dehydroxylation of clay micas was difficult due to the subtle transition between reactions. A small but definitive inflection point was used to establish the extrapolated dehydroxylation onset temperature. The inflection point of the fine clay was used to standardize the onset temperatures for the medium and coarse fractions. The small linear portion of the curve (at the inflection for the fine clay) was more sensitive to weight losses. The fine clay onset temperature served well for the other clays, falling in the linear portion for their respective inflection points. A second inflection point for the dehydroxlyation of the muscovite clays suggests that there are structural (OH) with different bonding energies. This is particularly true when considering that the fine clays contain significantly less interlayer K, and that water or H_3O may be coordinated in the interlayer. The temperature signifying completion of the dehydroxylation reaction was easily determined as the horizontal portion of the weight loss curve. Observed weight losses by muscovite clays were 7.1, 3.0, 3.2% (wt.) for the fine, medium and coarse fractions, respectively (Figure 19). Corresponding losses by biotite clays were 2.6, 1.1, and 0.5% (wt.), represented in Figure 20. The biotite clays showed weight gain

from 500 to 800°C, due to oxidation of octahedral Fe^{2+}. The fine clay biotite gained the least weight (0.1%), followed by the medium (0.25%) and then the coarse (0.5%) fractions. The oxidative weight gain for the biotite clays may partially obscure dehydroxylation, particularly, because dehydroxylation of the clays occurs at lower temperatutes than their macroscopic counterparts. The proposed mechanisms of dehydroxylation will be discussed subsequently.

At temperatures above 900°C micas recrystallize, the products being dependent on the species of mica. A small weight loss, observed at approximately 950°C has been attributed to the release of lattice strain (Eberhart, 1963). Depression of the reaction temperature due to reduced particle size was not observed for recrystallization, as it was for deydroxylation. Identification of recrystallization products was beyond the scope of this project. However, a brief summary of predicted recrystallization reactions is presented here. Muscovite recrystallization products have been determined to be; γ-Al_2O_3 above 980°C (Roy, 1949), or a spinel-like phase (Eberhart, 1963). Up to 1140°C, anhydrous muscovite should yield leucite, K-feldspar, and mullite (Brindley and Lemaitre, 1987). Roy (1949) found iron-rich spinel, leucite, and mullite recrystallization products for the conversion of biotite at 1100°C. Other potential reaction products for biotite are enstatite or forsterite and γ-Fe_2O_3. The formation of γ-Fe_2O_3 occurs *in situ* and does not exist as a separate phase from the biotite (Hogg and Meads, 1975). The rate and temperatures of dehydroxylation, and the oxidation of Fe-containing minerals is strongly influenced by the atmosphere used during analysis.

Brindley and Lemaitre indicate that the ideal recrystallization of micas also liberates excess silica, although experimentally none has yet been found. It should be noted that all of the aforementioned recrystallization products are extrapolated from equilibrium conditions, and as Yoder and Eugster (1955) indicated the recrystallization reactions of micas are nonequilibrium.

Surface area analysis

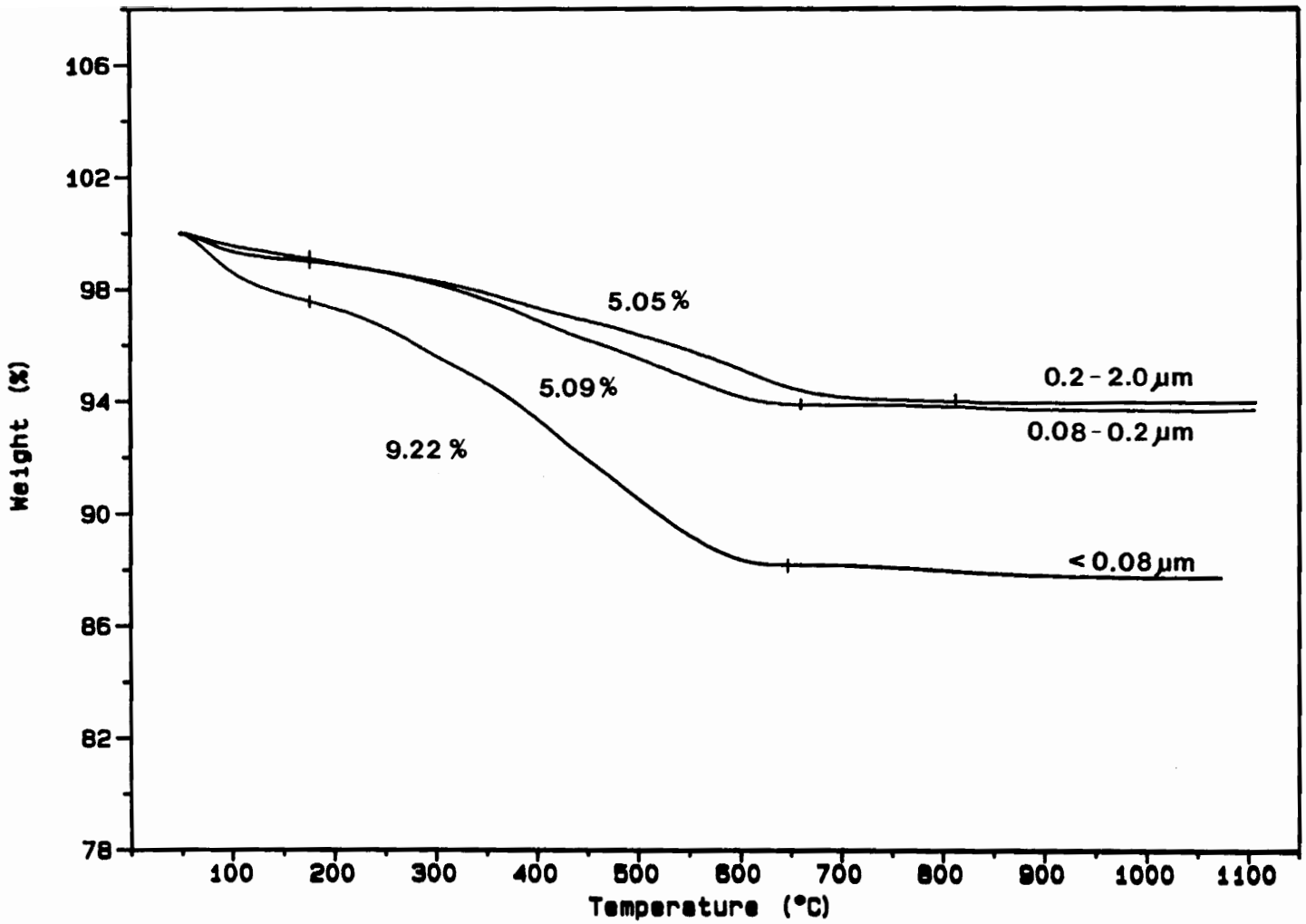

Figure 19. Composite thermogram of weight losses of muscovite clays due to desorption and dehydroxylation.

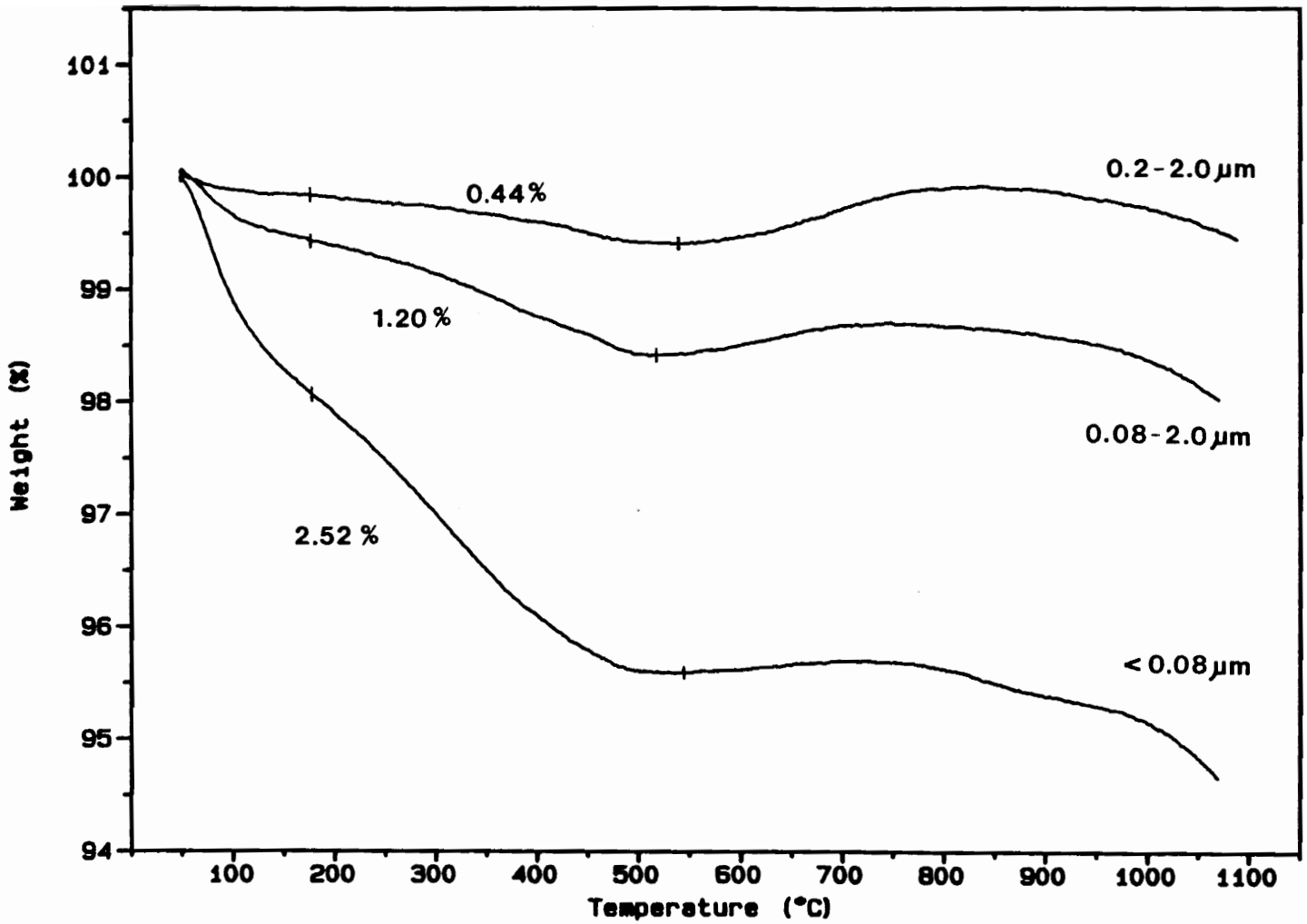

Figure 20. Composite thermogram of weight losses of biotite clays due to desorption and dehydroxylation.

The NH_4NO_3 saturated, salt free, clays were analyzed for specific surface area at liquid nitrogen temperatures, and surface areas determined by the monolayer adsorption of molecular nitrogen. Surface areas of the coarse, medium, and fine clay muscovite yielded values of 22.50, 74.67, and 91.38 m^2/g, respectively. Surface areas for the biotite clays were; 22.03, 84.89, and 150.65 m^2/g for coarse, medium and fine clays, respectively.

Ion exchange

Measurement of the small permanent charge on muscovite clays was difficult, especially, for coarse clays. The exchange capacity of these clays is dependent on the number of charged sites which are exposed to the reactant solution. The large permanent charge of muscovite is located at basal surfaces, where solution ions interact with the tetrahedral sheets. The pH dependent charge, usually assumed to be small, is allocated to the edges of particles. The edge charge arises from the charge deficiencies created by the breaking of bonds in both tetrahedral and octahedral sheets. The ability of solution ions to compensate for charge deficiencies may be enhanced for fine clays, due to the larger external surfaces. Charge deficiencies due to isomorphic substitution may be ameliorated by ion diffusion, because of the large surface area to volume ratio. Ion diffusion presupposes sufficient reaction time.

The NaCl saturated muscovite clays were exchanged with NH_4NO_3 The cation exchange for a constant charge mineral such as muscovite would be expected to be a small measureable charge, dependent on the number of wedge sites at particle edges. An unexpanded muscovite may have a CEC of <1 or as high as 10 meq/100 g. Typical values for the CEC of illite possessing expansible layers range between 10-40 meq/100 g. The exchange capacities of muscovite is due to isomorphic substitution, producing a permanent charge imbalance. The extent of the contribution to the total charge by pH dependent sites is unknown. However, the proportion of variable charge to total charge would be expected to be small, and would be located at particle edges. The comminution of the muscovite to produce clays produced a

large number of broken bonds, particularly at particle edges. The large number of Al-oxygen and Si-oxygen bonds at cleaved edges should provide numerous variable charge sites for proton interactions. The relativley small proportion of charge exposed at particle surfaces limits the anion exchange capacity of muscovite. The displacement of Cl^- ions by NO_3^- was negligible.

Exchange of the index cation Na increased linearly with increasing pH, for the medium clay muscovite. Sodium exchange in the 0.1N NaCl occurred over a much narrower range in pH, than in the 0.01N and 0.001N solutions (Figs. 21,22,23). The pH of the 0.1N NaCl solutions was much lower than the other salt concentrations. Solution protons may have acted as complementary ions in the exchange of Na by NH_4^+. The exchange of Na at low pH values may have involved partially hydrolyzed species at particle edges in addition to basally coordinated ions.

Potassium concentrations in both the reactant and exchange solutions suggest partial dissolution in all three clay sizes (Figs. 24,25,26). Several researchers have reported the inhibition of K exchange at very low solution concentrations. Rausell-Colom (1964) found that 4 ppm K in solution prevented exchange from some micas, while concentrations of 0.1 ppm were shown to inhibit exchange from muscovite to a maximum of 17% by Scott and Smith (1966). The amount of exchange is therefore dependent on the method of exchange, solution concentrations of K, and mica species. Despite release of K, possibly by partial dissolution, exchangeable levels appear to be pH independent. The exception to this trend is the 0.1N solution of the fine clay, in which exchangeable K increases with decreasing pH (Figure 24). Despite the confounding influence of proton concentrations, exchangeable K was similar for the three ionic strengths, ranging between 1.3 and 2.4 meq/100 grams. The low levels of exchangeable K for the three ionic strengths, suggest that removal is linked to the permanent charge charactersitics for all three clay sizes. If removal of interlayer K by protons occurs, the identity of the hydrogen species is of great interest. Interlayer spacing of unexpanded

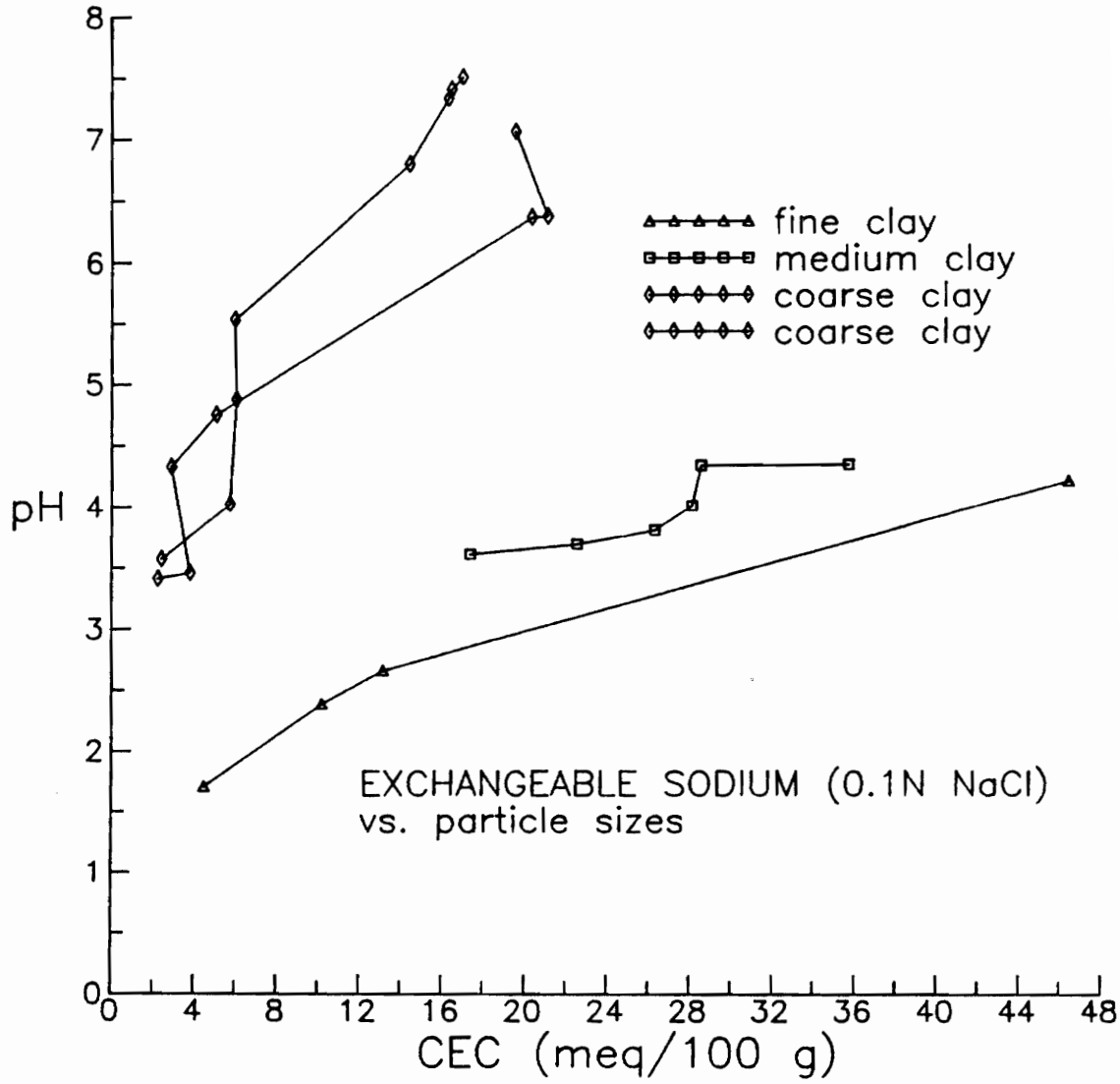

Figure 21. Composite cation exchange curve of Na^+ in 0.1N NaCl as influenced by the clay size of muscovite.

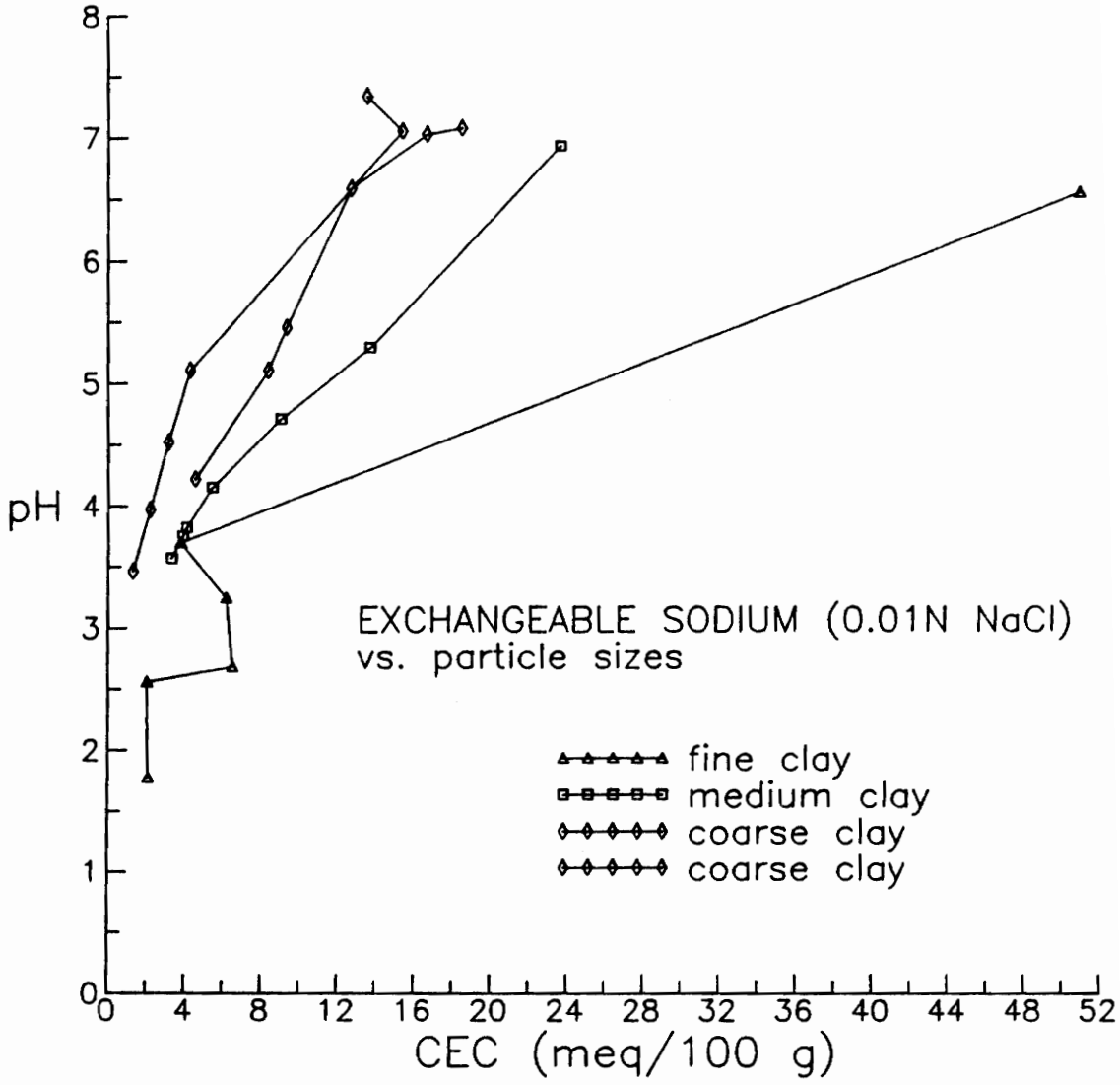

Figure 22. Composite cation exchange curve of Na^+ in 0.01N NaCl as influenced by the clay size of muscovite.

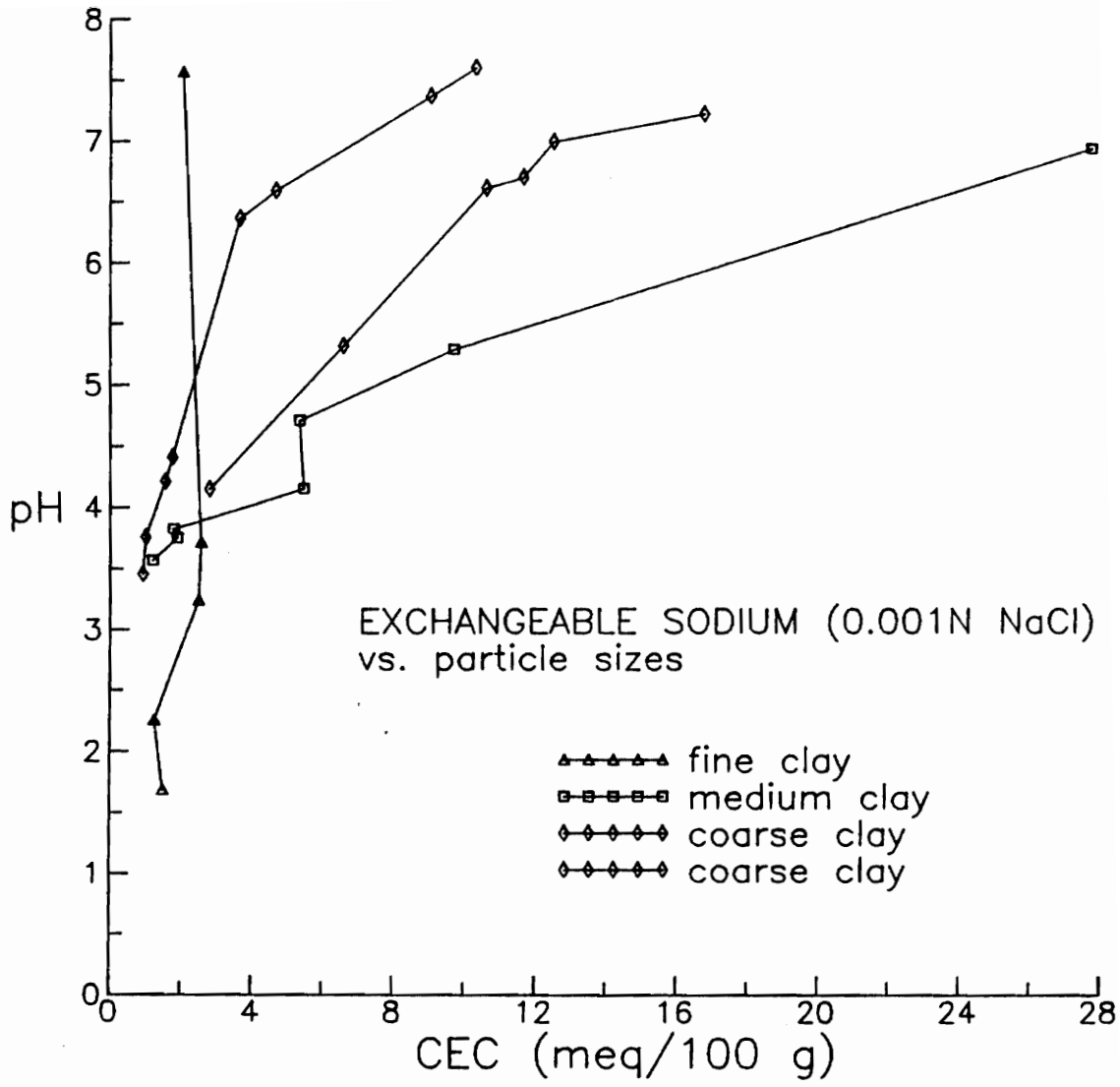

Figure 23. Composite cation exchange curve of Na^+ in 0.001N NaCl as influenced by the clay size of muscovite.

muscovite should limit the removal of K to either hydronium ions or discrete protons. Removal of K from expanded particle edges (wedge sites) may be readily effected by NH_4^+.

The fine clay muscovite, because of the very small particle size, readily released $Al^{3+}$and K. The release of K in the 0.1N solution was more clearly a dissolution, than in the 0.001N and 0.01N solutions. The released Kreached a maximum of 2.6 meq/100 g. Aluminum represented the largest portion of the cation activity for the fine clay, although its release was due to dissolution (Figs. 27,28,29). Exchangeable Na was much lower than expected for the fine clay, being less than that of the coarse and medium clays. The fine clay also released the largest amount of protons of the three particle sizes. The reduced levels of exchangeable Na, the large amount of Al^{3+}dissolution, and the relatively large quantity of hydrogen ion exchanged (Figs. 30,31,32) suggests that the fine clay was H^+ saturated. The hydrogen ion saturation of the fine clay may be attributed to the abundance of broken oxygen bonds at the particle edges, where proton coordination reduces charge

Plots of exchange curves for the index anion, Cl^-, indicate essentially no exchangeable anion activity. The enigmatic plots of anion exchange in the 0.1N NaCl solutions are shown in Figures 33, 34, and 35, may be linked to Al^{3+} hydrolysis.

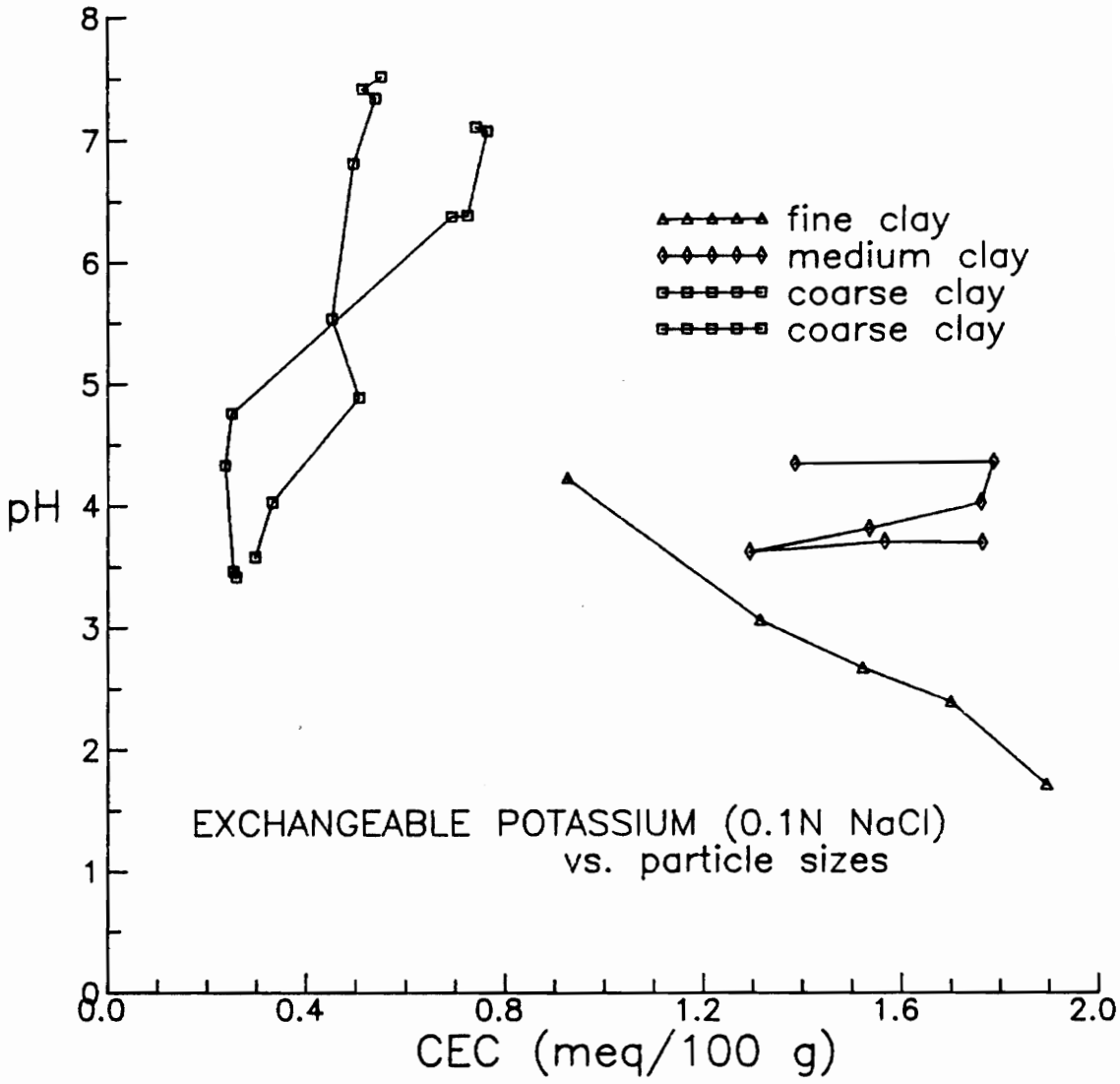

Figure 24. Composite cation exchange curve of interlayer K^+ in 0.1N NaCl as influenced by the clay size of muscovite.

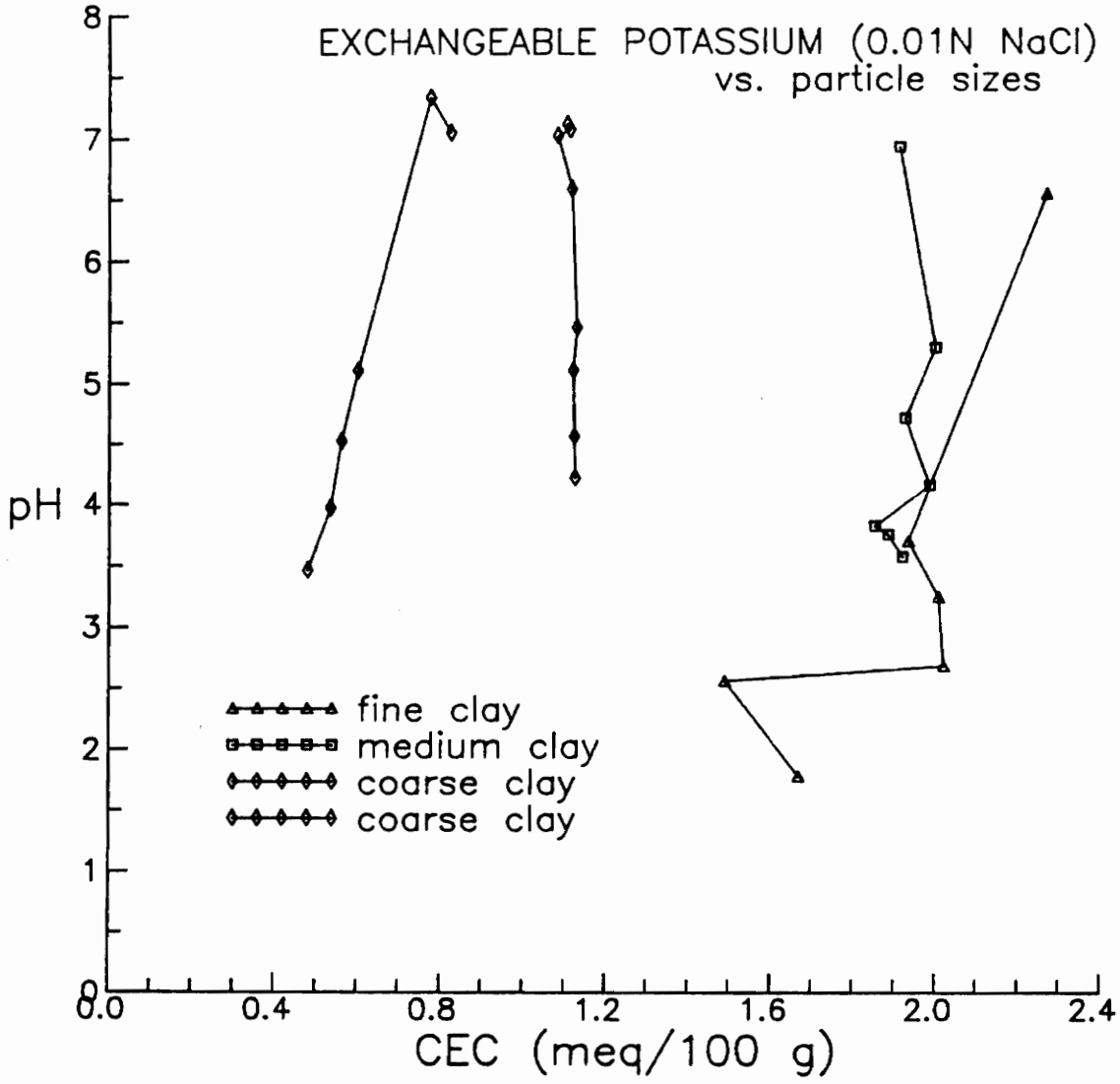

Figure 25. Composite cation exchange curve of interlayer K^+ in 0.01N NaCl as influenced by the clay size of muscovite.

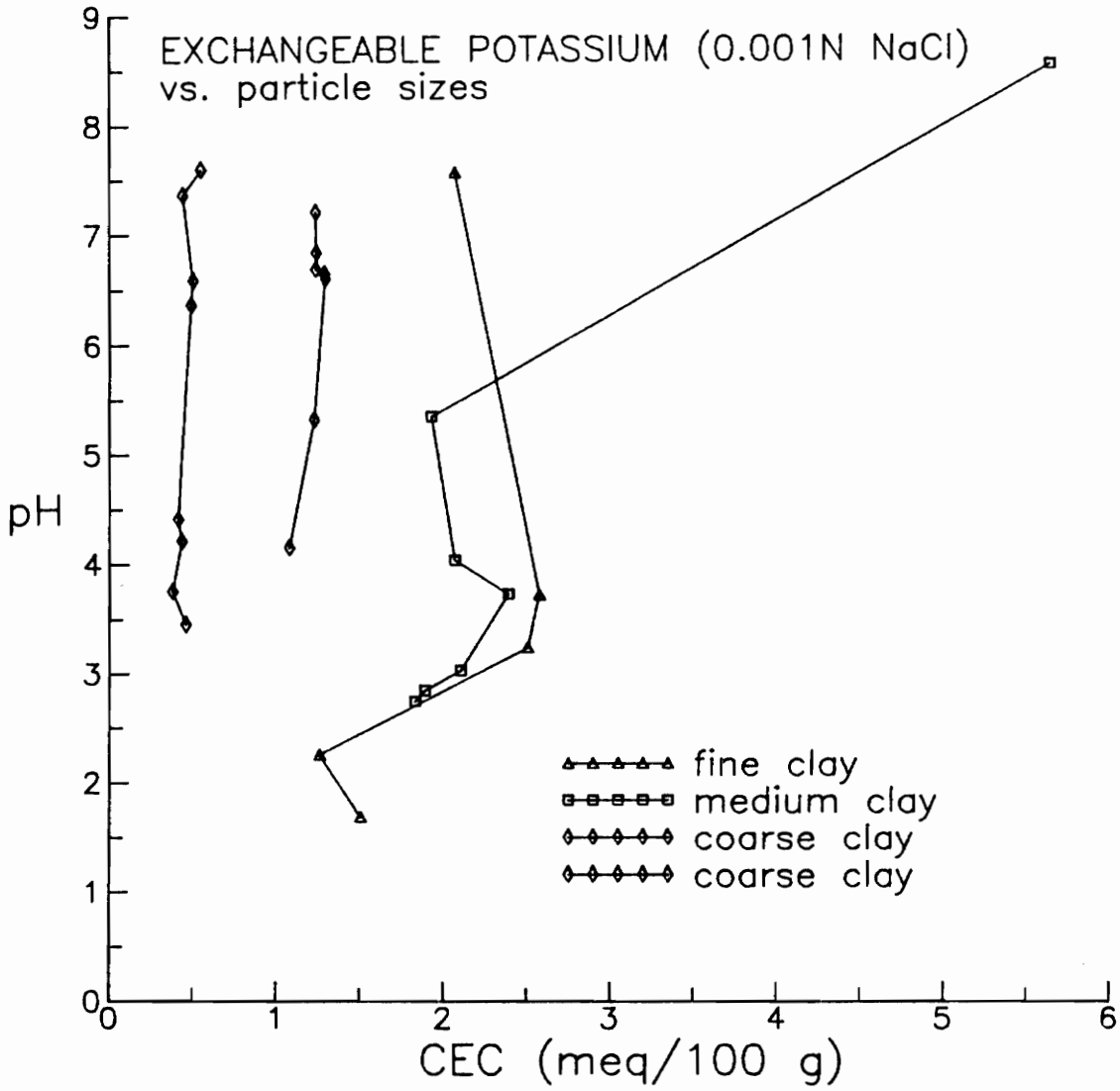

Figure 26. Composite cation exchange curve of interlayer K^+ in 0.001N NaCl as influenced by the clay size of muscovite.

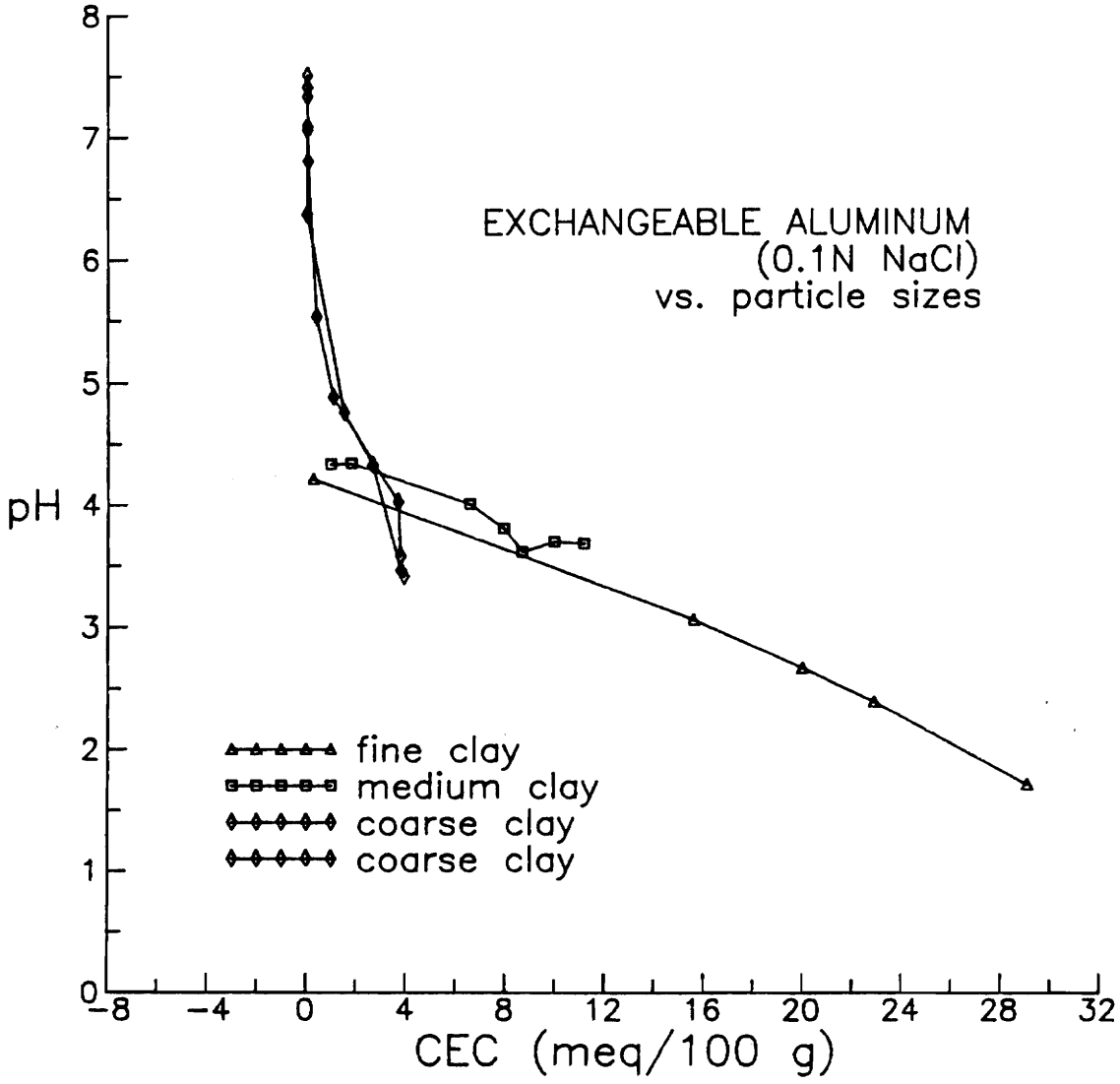

Figure 27. Composite cation exchange curve of Al^{3+} in 0.1N NaCl as influenced by the clay size of muscovite.

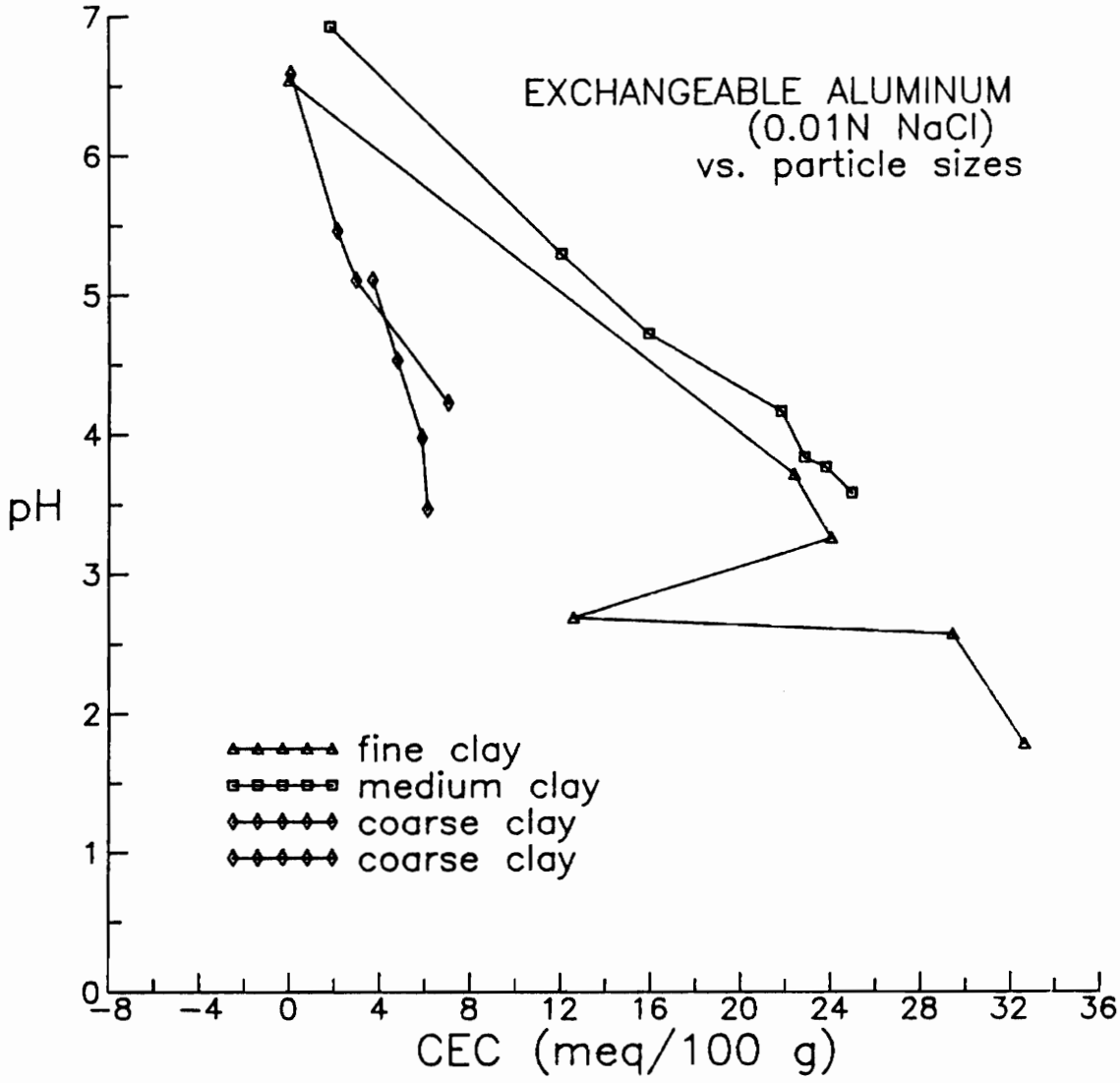

Figure 28. Composite cation exchange curve of Al^{3+} in 0.01N NaCl as influenced by the clay size of muscovite.

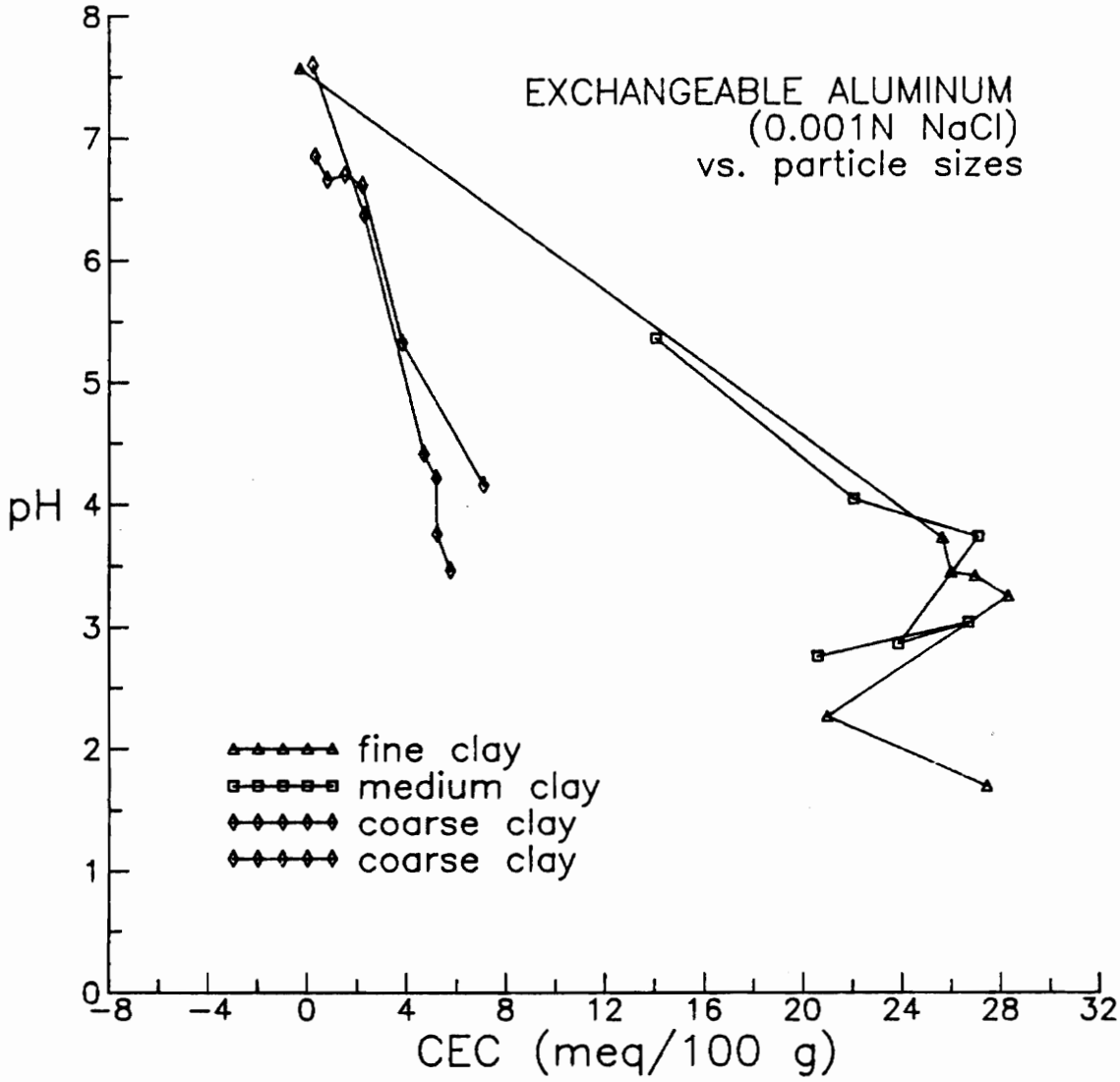

Figure 29. Composite cation exchange curve of Al^{3+} in 0.001N NaCl as influenced by the clay size of muscovite.

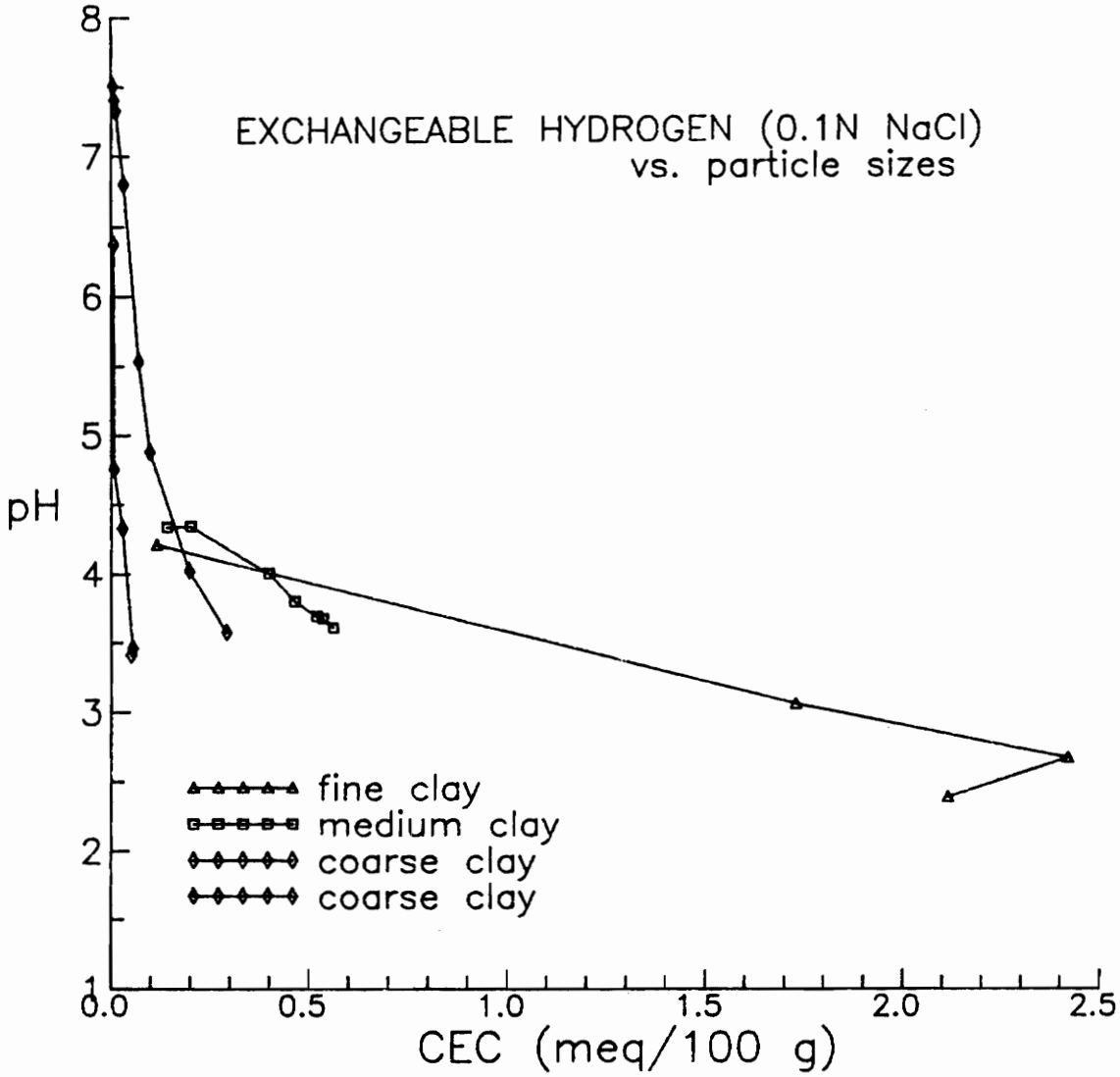

Figure 30. Composite cation exchange curve of "exchangeable" H^+ in 0.1N NaCl as influenced by the clay size of muscovite.

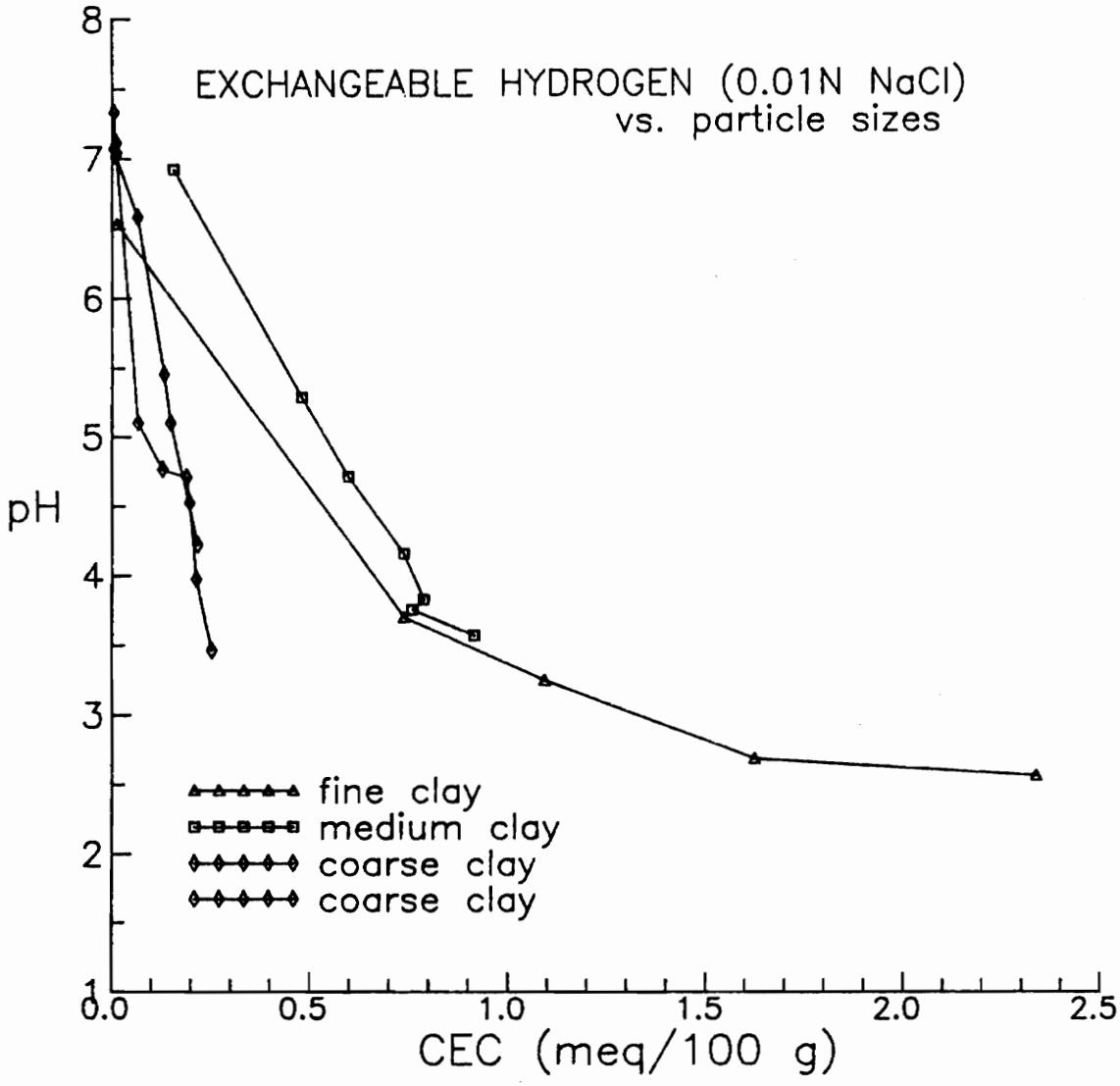

Figure 31. Composite cation exchange curve of "exchangeable" H^+ in 0.01N NaCl as influenced by the clay size of muscovite.

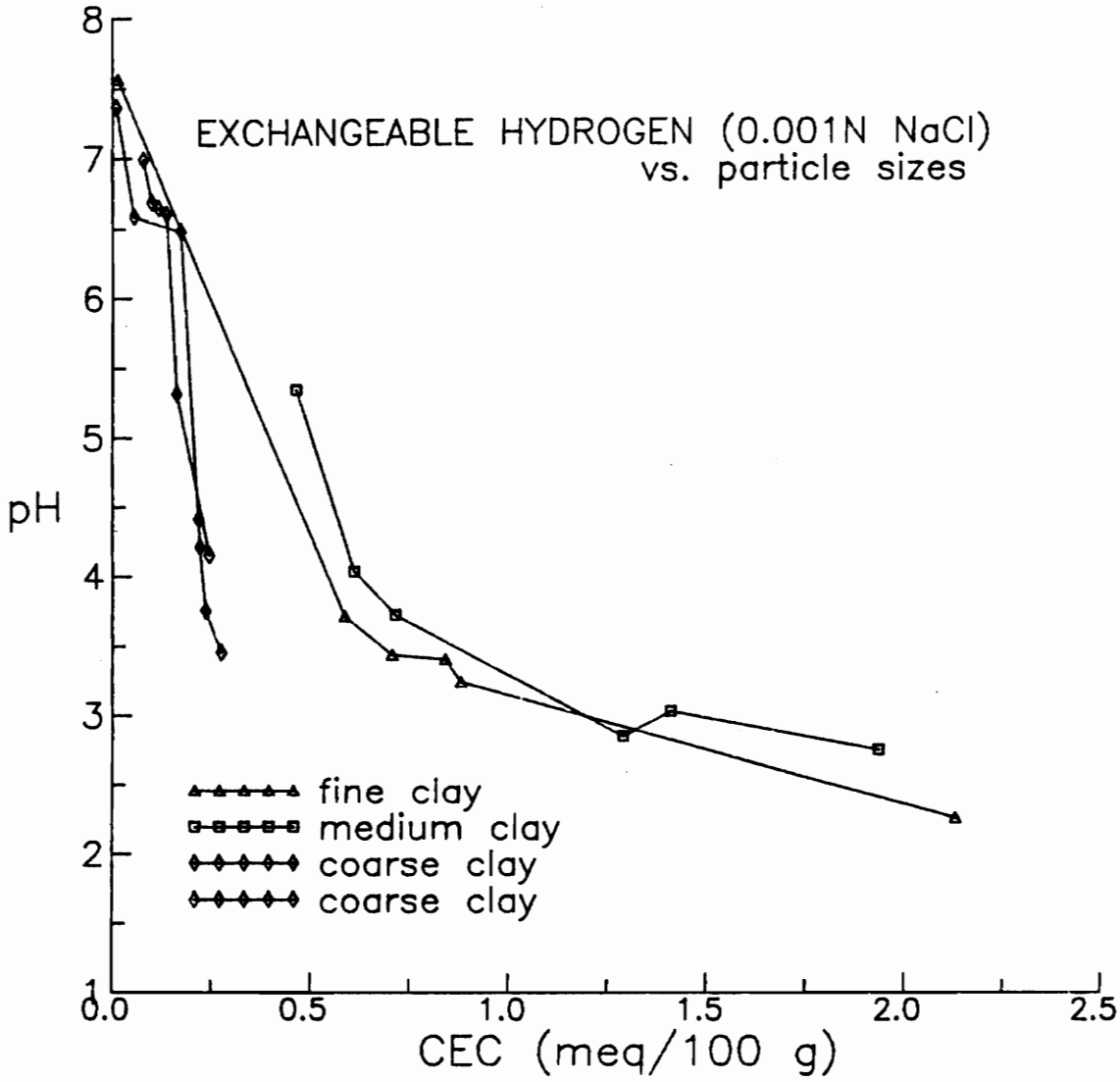

Figure 32. Composite cation exchange curve of "exchangeable" H^+ in 0.001N NaCl as influenced by the clay size of muscovite.

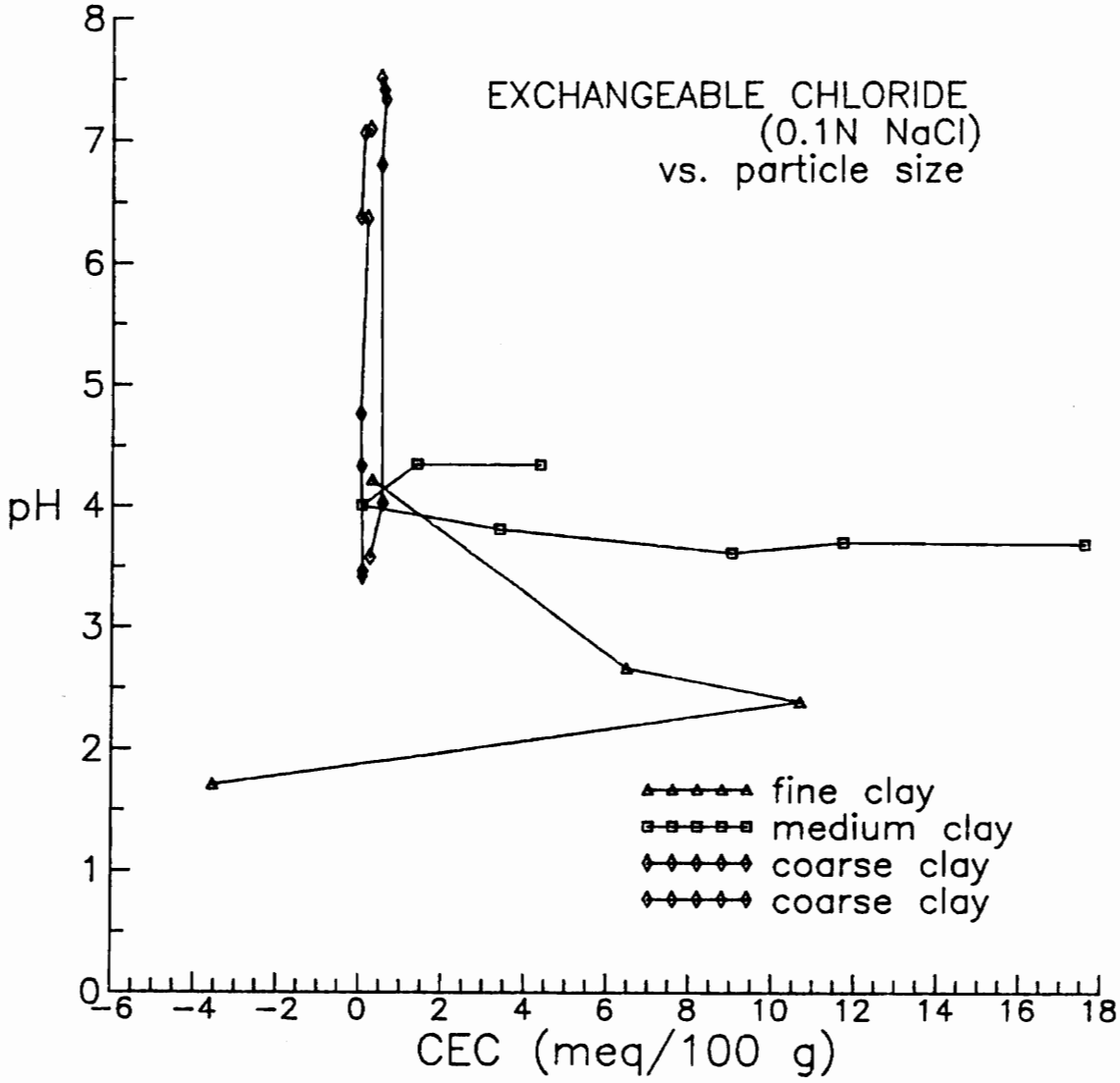

Figure 33. Composite anion exchange curve of Cl^- in 0.1N NaCl as influenced by the clay size of muscovite.

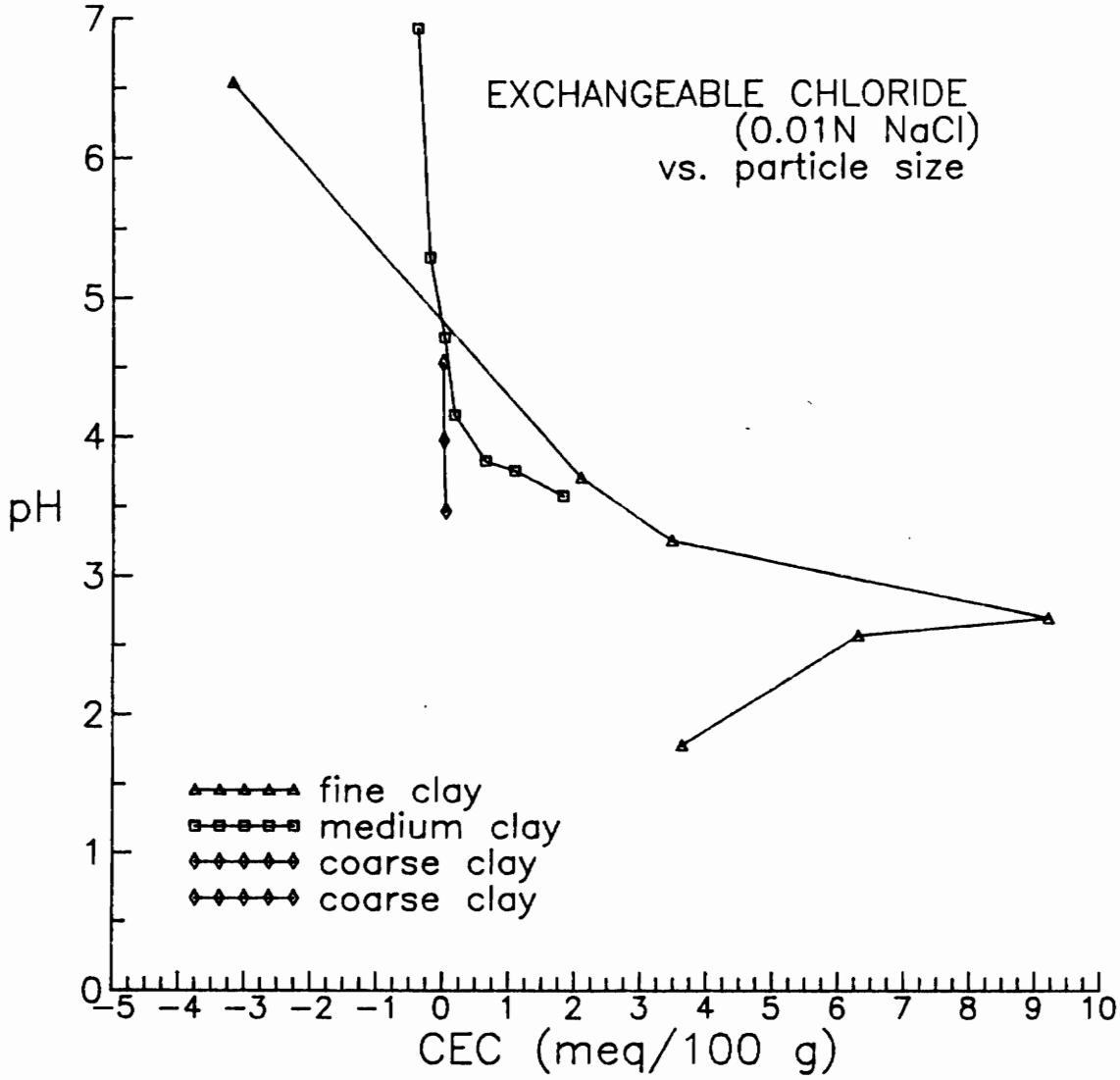

Figure 34. Composite anion exchange curve of Cl^- in 0.01N NaCl as influenced by the clay size of muscovite.

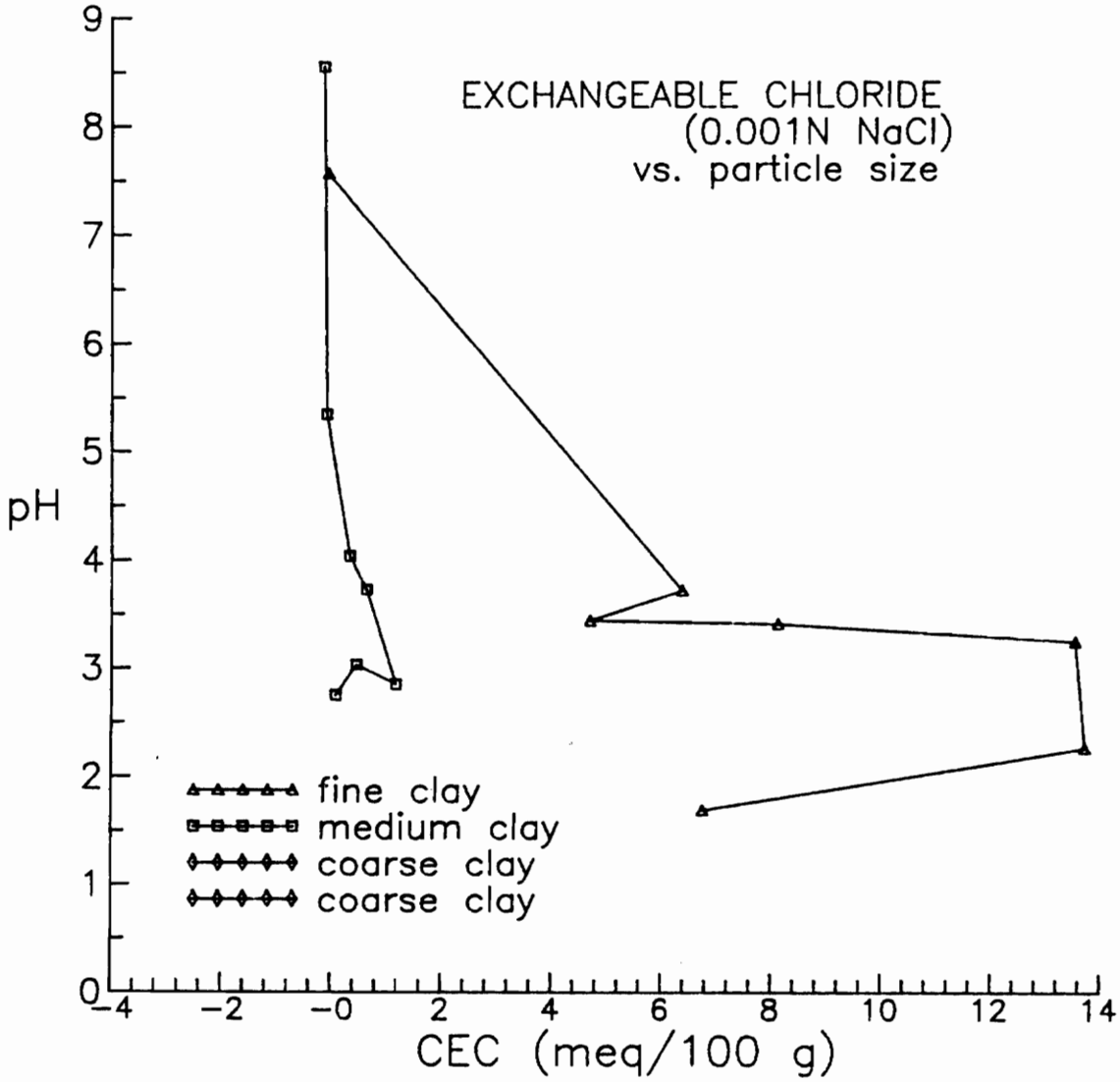

Figure 35. Composite anion exchange curve of Cl^- in 0.001N NaCl as influenced by the clay size of muscovite.

Chapter V

Discussion

Electron probe microanalysis

The analysis of the clays as bulk specimens presented a rigorous test of the capabilities of the instrument and its computerized data processing. Of paramount importance to reliable quantitation was the precise focusing of the electron beam at the surface of the clays. Due to the preparation of the filtered clays under vacuum a certain amount of preferred orientation was expected. However, the clays appeared as randomly oriented particles when viewed with the optics of the microprobe. The random particle orientation made precise focusing at the surface of the bulk specimen difficult.

Despite the inherent problems associated with analysis of bulk specimens, and the requisite ZAF corrections, there were no irregularities observed in elemental quantification of the fine (<0.08 μm), medium (0.08-0.2 μm), and coarse clays (0.2-2.0 μm). The use of a low accelerating potential (15 kV) eliminated problems associated with the diffusion of low atomic weight elements. The slightly lower concentration of Kand Na found in the fine clays was in accord

with the predicted behavior. The vigorous comminution required to produce the fine clays removed the susceptable cations in the interlayer, as well as octahedral Mg from the biotites and tetrahedral $Al^{3+}$from the muscovites. Quantification of elements occuring at lower abundances within the clays was enhanced by the use of long counting times. The infinitely thick filter cakes of clay eliminated problems associated with the x-ray emission from the substrate. However, there may have been particle shape effects on the x-ray pathlength component of the absorption function. The confounding influence of small particle size on the x-ray depth distribution was minimized due to the comparitively small differences between the sizes of the clays. With the exception of the fine clays which contain a relative abundance of lath shaped particles, the particle shape effects would be unimportant in the comparison of the clay analyses. Application of the theoretical particle size and particle shape models of Armstrong and Buseck (1975) would be neccesary to establish the shortcomings of this protocol and the validity of between clay comparisons. The excellent agreement of the clay analyses with those of the sheet material suggest that the conventional correction factors were adequate.

Transmission electron microscopy

The mechanical production of the biotite and muscovite clays imparted certain morphologic patterns to the particles. The medium and coarse clays of both minerals possess the typical angular morpholgy when viewed normal to basal planes. The progressive shearing of particles normal to (001) planes can be seen in the production of lath shaped particles. The seemingly random cutting of the mica particles may have been strongly influenced by structural and compositional properties of the minerals. Laths are much more abundant in the dioctahedral muscovite, particularly in the fine clay fraction. The cutting of the octahedral sheet in muscovite may provide preferred zones of weakness, where octahedral vacancies occur. These zones of weakness may enable the shearing of the particle while allowing the fragments to retain coherence of crystallinity. There was no decrease in weight percent Al^{3+}

allocated to octahedral positions by SuperRecal, for the muscovite clays. Cutting of trioctahedral biotite may be facilitated by tetrahedral substitutions, however, the significantly lowered Mg^{2+} content of the fine biotite clay attests to octahedral shearing. The proposed resilience of biotites to shearing normal to basal planes may predispose particles to cutting parallel to basal planes, previously described as stripping or delamination of tetrahedral sheets. Delaminated biotite fragments were not identified by XRD, however, these fragments may compose the finely divided particles found by TEM in the fine clay fraction. Further work with SAD analysis of the biotite clays would be needed to provide evidence to support this proposal.

X-ray diffraction

The clay fractions of both muscovite and biotite possess similar x-ray diffraction characteristics and particle morphologies. The fine clay fractions of both minerals are dominated by lath shaped particles. The fine particle size causes the diffraction peaks to to be very broad, low angle skewed and have low intensity. Definition of peak shape and position for these fractions was inconclusive. The medium and coarse fractions of the biotite and muscovite were composed primarily of angular and fan shaped particles, with minor amounts of laths. Both the medium and coarse clay fractions of biotite showed decreasing basal spacing with heating. The intermittent intensification of basal peaks for the medium and coarse biotites at 300°C may be attributed to the expansion of the unit cell by Fe^{2+} oxidation. The oxidation of Fe^{2+} distorts lattice dimensions, particularly along the *b* dimension. The loss of peak intensities at 550°C may be ascribed to higher Fe^{3+} concentrations causing disruption of the structures. The intensity of the 10Å peak for the medium and coarse muscovite generally decreases with heating. Interestingly, the 3.33A peak for the medium and coarse muscovite is enhanced by heating. Also of note is the occurence of several higher order reflections in the medium and coarse muscovite, at all temperatures. The presence of higher order re-

flections in all heat treatments suggests that particle shapes are responsible for these diffraction maxima.

Thermal analysis

The reaction of primary interest in TGA analysis of mica clays was intermediate temperature (150-550°C) dehydroxylation (dehydration). Oxidation of Fe^{2+} in the biotite clays was of considerable importance with respect to analysis of dehydroxylation reactions.

Dehydroxylation of clays is thought to be initiated by the dissociation of a proton from an (OH) group, with subsequent reaction to form water. The proton is described as being delocalized with respect to the oxygen atom. The decreased (OH) bonding has been detected by reduced absorption bands using infrared spectroscopy (Vedder, 1964; Fripiat et al., 1965). The interaction of the delocalized proton with an (OH) group to form water is thought to occur via either of two mechanisms. Reaction of the dissociated proton with an adjacent (OH) group has been described as a homogeneous reaction (Pampuch, 1971). The water molecule thus formed must move to a gas-solid interface to volatilize. Diffusion of the water molecule would require more energy than diffusion of a proton. The migration of a proton to a reaction zone, however, neccesitates counter migration of cations to maintain electrostatic neutrality. Proton migration and subsequent water formation at a reaction zone was originally coined by Ball and Taylor (1961) for dehydration of brucite.

Vedder and Wilkins (1969) and Rouxhet (1970) attribute the dehydroxylation and deuterium exchange reactions for several micas to be diffusion controlled. Using infrared spectroscopy and deuteration they proposed that diffusion in the micas occurred normal to the (001) plane. The mechanism of dehydration of clay size micas may be less constrained regarding structural controls on diffusion and dehydration, than their macroscopic counterparts. The decreased particle size of the clays may not only decrease the temperatures of dehydration but

also the energy levels required to initiate diffusion. Additionally, the altered composition of the clays may reduce the structural constraints on diffusion controlled dehydration. Eberhart (1963), Nicol (1964), and Vedder and Wilkins (1969) have shown that dehydroxylation of muscovite increases the unit cell dimensions. The proposal by Vedder and Wilkins is that dimensional changes are due to partial relaxation of the (Si,Al)-O bonds. Movement of the "residual" oxygen to the plane of the octahedral Al^{3+} was offered as a mechanism for unit cell expansion (Eberhart, 1963).

Homogeneous dehydroxylation seem to be the favored mechanism of dehydration of micas. Infrared analysis of rehydration by dehydrated muscovite and the apparent restoration of the structure led Vedder and Wilkins (1969) to consider dehydroxylation a homogeneous reaction. More recently, Mackenzie et al. (1987) used high resolution NMR to study dehydroxylation of two muscovites. These authors also favor a homogeneous dehydroxylation reaction.

The minor weight gain exhibited by oxidation of the fine biotite clay (0.1%) masks the presence of a slightly increased Fe content by EPMA. Similarly, the medium clay contains slightly more Fe than the coarse clay and yet it also had a smaller weight gain (0.25% vs. 0.5%). The suggestion is made here that oxidation of Fe^{2+} occurs simultaneously with dehydroxylation, yet its effects are masked by the magnitude of hydroxyl losses. It is also possible that Fe contents determined by EPMA may be artificially high due to contamination during sample preparation, as previously discussed.

Surface area analysis

The surface areas for the clays were smaller than expected, especially, considering the large amount of energy required to mechanically grind the material to clay size. The coarse clays possess nearly identical surface areas of 22.5 and 22.0 m^2/g for muscovite and biotite, respectively. A three to four fold increase in surface area was observed as particle size de-

creased from coarse to medium clays, biotite possessing a moderately larger area. Similarly, the increase in surface area as particle size decreased to fine clay was larger for the biotite. Biotite surface area nearly doubled between the medium and fine clays, increasing from 84.89 to 150.65 m^2/g. Comparably, the change in surface area between the medium and fine muscovite was nominally increased from 74.67 to 91.38 m^2/g. The proportionally larger surface area of the fine biotite may be due to the stripping of tetrahedral sheets from the 2:1 layers, and possibly to the production of noncrystalline material. Electron micrographs for the fine biotite clay shows abundant material of very small size and of unknown crystallinity. The single SAD micrograph of a well crystalline particle did not provide any evidence of tetrahedral stripping.

Analysis of particle height distributions for the fine clays corroborates the surface area determination, with the fine biotite having over 94% of particles below 0.02 μm height. Fine muscovite clay had fewer particles (43%) below this height. The strong skewness of the fine biotite explains the dramatically larger surface area relative to muscovite. Similar conclusions may be drawn regarding the medium clays, although the differences are smaller. Particle heights for the coarse clays did not exhibit skewness. Basal areas for the clays did not support a correlation to surface areas, basal areas being centrally located within designated ranges for all three clay sizes.

Ion exchange

Overestimation of the amount of H^+ needed to obtain the desired solution pHs for exchange caused dissolution, which confounded the CEC and AEC determinations. Generally, cation exchange increased with ionic strengths, decreasing particle size, and higher pH values.

The small positive anion exchange for the 0.01N and 0.001N NaCl solutions conforms to the predicted anion exclusion by double layer theory. The anomolous anion exchange of the 0.1N

NaCl solutions has not enabled correlation to predicted behavior, nor correlation to the empirical behavior of the other ionic strengths.

The role of Kin the cation exchange reactions appears to be largely pH independent, however the determination of the nature and mechanisms of Krelease are uncertain. Perhaps a column study would enable the separation of kinetic effects, and elution profiles may distinguish between exchange and dissolution more readily than this batch study.

The concentrations of Al^{3+} exchanged indicate the susceptability of muscovite to dissolution, even in dilute salt solutions. Congruent dissolution of muscovite was found by 't Serstevens et al. (1978) at high solution pHs and at low pHs after partially hydrolyzed Al^{3+} was stripped from the mica surface. These authors attributed the surface accumulation of Al^{3+} on muscovite to be due to combined K-hydrolysis and Si dissolution. They also present evidence of ionic strength suppression of K-hydrolysis, which is consistent with the findings presented here. Data from this investigation suggests that partially hydrolyzed Al^{3+} was released to the acidified NaCl solution and protons became potential determining. The transition of the protons acting as potential determining ions to becoming active in particle dissolution may have been dependent on the number of broken O bonds at particle edges. Fine clays, while providing the largest surface areas for solution interaction may also have been able to coordinate more solution protons without dissolution, due to the large proportion of broken O bonds. Solution Al^{3+} competed with protons for unsatisfied edge sites down to pH 4. Between pH 3 and pH 4 Al^{3+} hydrolyzes, therefore hydrolysis products may also compete for charged sites on the clay surfaces. The fine clay muscovite preferred protons as the means of charge balance, possessing a relatively large amount of exchangeable H^+. The edges of the fine clay muscovite may have been H^+ saturated. The relative abundance of H^+ and the slightly lower tetrahedral Al^{3+} content by EPMA, suggests that some Al^{3+} was removed from this clay fraction due to grinding.

Conclusion

The compositions of the medium and coarse clays of muscovite and biotite were little changed by mechanical grinding, from the compositions of the original sheet materials. The medium and coarse clays exhibited strong and coherent x-ray diffraction maxima, consistent with macroscopic mica samples. Particle morphologies for the larger clays were also consistent with those of macroscopic specimens. The specific surface areas of the coarse and medium clays were correlated well with the amounts of coordinated water, determined by thermogravimetric analysis.

Fine clays, of biotite and muscovite, were of significantly different elemental compositions than the larger clays, and also the sheet materials. The interlayer cations of both fine clay fractions were the most susceptable to removal by grinding. Loss of interlayer K from fine clay muscovite was accompanied by a decrease in tetrahedral Al, and increased octahedral Al. Whether removal of tetrahedral Al^{3+} was effected by the grinding, or whether separation of 2:1 layers during grinding caused K removal and subsequent charge relocation is not discernable by this study. The increase of Fe in the fine clay biotite is not understood in terms of the magnitude of weight gain during thermal analysis, nor by the presence of the second order 5Å diffraction peak. The oxidative weight gain of the fine biotite may have been masked by the dehydroxylation reactions, which are of significantly greater magnitude.

Diffraction characteristics of the fine clays were significantly affected, exhibiting poorly resolved basal reflections. The peak maxima were of very low intensity and extremely broad. The degree of crystallinity of the fine clays were reduced during their preparation, yet particles exhibited coherence by transmission electron microscopic examination. This perceptual difference is due to the much better resolving power of the shorter wavelength electron beam.

The measurement of the small exchangeable charge on the clay size muscovite and biotite was confounded by protocol difficulties. However, observed trends were in accord with predicted increases in exchange capacity with decreasing particle size, and increasing ionic strength. There was also an apparent increase in pH dependent charge with decreasing particle size, as more broken O bonds at particle edges interact with potential determining ions in solution.

Literature Cited

Ahn, J.H., D.R. Peacor, and E.J. Essene. 1986. Cation-diffusion-induced characteristic beam damage in transmission electron microscopic images of micas. Ultramicroscopy, *19*:375-382.

Albee, A.L., and L. Ray. 1970. Correction factors for electron probe microanalysis of silicates, oxides, carbonates, phosphates, and sulfates. Anal. Chem. *42*(12):1408-1414.

Armstrong, J.T., and P.R. Buseck. 1975. Quantitative chemical analysis of individual microparticles using the electron microprobe:Theoretical. Anal. Chem. *47*(13):2178-2192.

Ball, M.C., and H.F.W. Taylor. 1961. Dehydration of brucite. Mineral. Mag. *32*:754-766.

Bates, T.F. 1964. The application of electron microscopy in soil clay mineralogy. *In* Rich and Kunze (ed.) Soil clay mineralogy. Univ. North Carolina Press, Chapel Hill. 125-147.

Baweja, A.S., L.P. Wilding, and E.O. McLean. 1974. Mineralogy and cation exchange properties of libby vermiculite separates as affected by particle-size reduction. Clays Clay Miner. *22*:253-262.

Bence, A.E., and A.L. Albee. 1968. Empirical correction factors for the electron microanalysis of silicates and oxides. J. Geol. *76*:382-403.

Beutelspacher, H., and H.W. van der Marel. 1968. Atlas of electron microscopy of clay mineral and their admixtures. Elsevier Publishing Co., Amsterdam.

Bloss, F.D., 1959. Mica hardness due to F content. Am. Miner. *44*:33-48.

Bowen, L.H., S.B. Weed, and J.G. Stevens. 1969. Mossbauer study of micas and their potassium-depleted products. Am. Mineral. *54*:72-84.

Bradley, W.F., and R.E. Grim. 1951. The mica clay minerals. Am. Miner. *36*:182-201. ✓ SY

Brown, G. and G.W. Brindley. 1980. X-ray diffraction procedures for clay mineral identification. p. 305-359. *In* G.W.Brindley and Brown (ed.) Crystal structures of clay minerals and their x-ray identification. Mineralogical Soc. G. Br. QE 35

Brindley, G.W., and J. Lemaitre. 1987. Thermal, oxidation and reduction reactions of clay minerals. p. 319-370. *In* Chemistry of clays and clay minerals. Mineralogical Soc. G. Br.

Brunauer, S., P.H. Emmett, and E. Teller. 1938. Adsorption of gases in multimolecular layers. J. Am. Chem. Soc. *60*:309-319.

Chute, J.H., and J.P. Quirk. 1967. Diffusion of potassium from mica-like clay minerals. Nature (London) *221*:1156-1157.

Cook, M.G., and C.I. Rich. 1963. Negative charge of dioctahedral micas as related to weathering. p. 47-63. *In* Eleventh National Conference on Clays and Clay Minerals.

Cullity, B.D., 1978. Elements of x-ray diffraction, 2nd ed. Addison-Wesley Publishing, Reading, MS.

Eberhart, J.P., 1963. Transformation du mica en muscovite par chauffage entre 700 et 1200°C. Bull. Soc. franc. Miner. Cristallogr. *86*:213-251.

Fanning, D.S., and V.Z. Keramidas. 1977. Micas. p.195-258. *In* Minerals in soil environments. Soil Sci. Soc. Am., Madison, WI.

Feigenbaum, S., R. Edelstein, and I. Shainberg. 1981. Release rate of potassium and structural cations from micas to ion exchangers in dilute solutions. Soil Sci. Soc. Am. J. *45*:501-506.

Fripiat, J.J, P.G. Rouxhet, and H. Jacobs. 1965. Proton delocalization in micas. Am. Miner. *50*:1937-1958.

Grim, R.E. 1968. Clay mineralogy. 2nd ed. McGraw-Hill, New York.

Heidenreich, R.H. 1964. Fundamentals of transmission electron microscopy. Interscience Publishers, New York.

Heinrich, K.F.J. 1981. Electron beam x-ray microanalysis. Van Nostrand Reinhold Co. New York.

Hogg, C.S., and R.E. Meads. 1975. A mossbauer study of thermal decomposition of biotites. Mineral. Mag. *40*:79-88.

Huff, W.D. 1972. Morphological effects on illite as a result of potassium depletion. Clays Clay Miner. *20*:295-301.

Jackson, M.L. 1969. Soil chemical analysis-Advanced course. Published by author, Dept. Soil Science, Univ. of Wisconsin, Madison, WI.

Johansson, E., S. Wold, and K. Sjodin. 1984. Minimizing effects of closure on analytical data. Anal. Chem. *56*:1685-1688.

Langmuir, I. 1918. The adsorption of gases on plane surfaces of glass, mica and platinum. J. Am. Chem. Soc. *40*:1361-1402.

Laverdiere, M.R., and R.M. Weaver. 1977. Charge characteristics of spodic horizons. Soil Sci. Soc. Am. J. *41*:505-510.

LeRoux, J., and C.I. Rich. 1969. Ion selectivity of micas as influenced by degree of potassium depletion. Soil Sci. Soc. Am. Proc. *33*:684-689.

Lin, F.C., and C.V. Clemency. 1981. The kinetics of dissolution of muscovites at 25°C and 1 atm CO_2 partial pressure. Geochem. Cosmochem. Acta *45*:571-576.

Mackenzie, K.J.D., I.W.M. Brown, C.M. Cardile, and R.H. Meinhold. 1987. The thermal reactions of muscovite studied by high-resolution solid-state ^{29}-Si and ^{27}-Al^{3} NMR. J. Amer. Ceram. Soc. *70*:2645-2654.

Mackenzie, R.C. (ed.), 1970. Differential thermal analysis. Vol. 1, fundamental aspects. Academic Press, New York.

Mackenzie, R.C., and A.A. Milne. 1951. The effects of grinding on micas. Clay Miner. Bull. *2*:57-62.

Mackenzie, R.C., and A.A. Milne. 1953. The effects of grinding on micas. I.Muscovite. Mineral. Mag. *30*:178-185.

Mackinnon, I.D.R. and S.A. Kaser. 1987. Microanalysis of clays at low temperature. Microbeam Analysis p. 332-334.

Mortland, M.M. 1958. Kinetics of potassium release from biotite. Soil Sci. Soc. Am. Proc. *22*:503-508.

Newman, A.C.D., and G. Brown. 1969. Delayed exchange of potassium from some edges of mica flakes. Nature (London) *223*:175-176.

Newman, A.C.D., 1970. The synergetic effect of hydrogen ions on the cation exchange of potassium in micas. Clay Minerals *8*:361-373.

Nicol, A.W. 1964. Topotactic transformation of muscovite under mild hydrothermal conditions. Clays Clay Miner. *12*:11-19.

Pampuch, R. 1971. Le mecanisme de la deshydroxylation des hydroxydes et des silicates phylliteux. Bull. Grpe. franc. Argiles *23*:107-118.

Raman, K.V., and M.L. Jackson. 1965. Mica cleavage morphology changes during potassium release and fixation. J. Indian Soc. Soil Sci. *13*:65-69.

Raman, K.V., and M.L. Jackson. 1966. Layer charge relations in clay minerals of micaceous soils and sediments. p. 53-68. *In* Fourteenth National Conference on Clays and Clay Minerals.

Rausell-Colom, J.A, T.R. Sweatman, C.B. Wells, and K. Norrish. 1964. Studies in the artificial weathering of mica. p. 40-72. *In* E.G. Hallsworth and D.V. Crawford (ed.) Experimental Pedology. Univ. of Nottingham. Butterworths, London.

Rich, C.I. and R.I. Barnhisel. 1977. Preparation of clay samples for x-ray diffraction analysis. p. 797-808. *In* J.B. Dixon and S.B. Weed (ed.) Minerals in soil environments. SSSA, Madison, WI.

Rouxhet, P.G. 1970. Kinetics of dehydroxylation and of OH-OD exchange in macrocrystalline micas. Am. Mineral. *55*:841-853.

Roy, R. 1949. Decomposition and resynthesis of micas. J. Am. Ceramic Soc. *32*:202-209.

Scott, A.D. and S.J. Smith, 1966. Susceptability of interlayer potassium in micas to exchange with sodium. p. 69-81. *In* Fourteenth National Conference on Clays and Clay Minerals. Pergamon Press, New York.

't Serstevens, A., P.G. Rouxhet, and A.J. Herbillon. 1978. Alteration of mica surfaces by water and solutions. Clay Miner. *13*:401-409.

Suito, E., and M. Nakahira. 1971. Mica and related minerals. p. 231-234. *In* J.A. Gard (ed.) Electron-optical investigation of clays. Mineral. Soc G. Br.

Switzer, G., 1941. Hardness of micaceous minerals. Am. J. Sci. *239* p.316.

Tanner, C.B. and M.L. Jackson, 1947. Nomographs of sedimentation times for soil particles under gravity or centrifugal acceleration. Soil Sci. Soc. Proc. *11*:60-65.

Van der Pluijm, B.A., J.H. Lee, and D.R. Peacor. 1988. Analytical electron microscopy and the problem of potassium diffusion. Clays Clay Miner. *36*:498-504.

Vedder, W. 1964. Correlation between infrared spectrum and chemical composition of mica. Am. Mineral. *49*:736-768.

Vedder, W., and R.W.T. Wilkins. 1969. Dehydroxylation and rehydroxylation, oxidation and reduction of micas. Am. Mineral. *54*:482-509.

von Reichenbach, H. Graf and C.I. Rich. 1969. Potassium release from muscovite as influenced by particle size. Clays Clay Miner. *17*:23-29.

Wells, C.B., and K. Norrish. 1968. Accelerated rates of release of interlayer potassium from micas. *2*:683-694. *In* Trans. 9th Int. Congr. Soil Sci.

Yoder, H.S. and H.P. Eugster, 1955. Synthetic and natural muscovites. Geochim. Cosmochim. Acta. *8*:225-280.

Ziebold, T.O., and R.E. Ogilvie. 1964. An empirical method for electron microanalysis. Anal. Chem. *36*:322-327.

Vita

of

Paul Lawrence Gassman

Paul Lawrence Gassman was born September 14, 1956 in Homestead, Florida. He graduated from Paint Branch High School, Burtonsville, Maryland in August of 1973. Paul met Carol Stapleton after relocating in northern Virginia, and in June of 1978 they were married. In August, 1979, Paul earned an associate in science degree (Geology) from Northern Virginia Community College. He then transferred to Virginia Polytechnic University and State University, and earned a bachelor of science degree in Geology in August, 1983. In June of 1984, Paul began employment as a Laboratory Specialist in the Agronomy Department at VPI & S.U., and the following September began his part-time graduate studies in Soil Science (clay mineralogy and soil chemistry). The requirements for a master of science degree, in Soil Science, in the Department of Crops and Soil Environmental Sciences (formerly the Agronomy Department) were completed in February, 1990.